Table 1
Echocardiographic measurements in TAC- and sham-operated mice with or without treatment with cromolyn

	Sham		TAC	
Cromolyn	(–)	(+)	(–)	(+)
Number	10	5	17	15
HW/BW (mg/g)	4.55 ± 0.11	4.64 ± 0.04	5.24 ± 0.05[A]	5.54 ± 0.13[A]
HR (bpm)	610.10 ± 7.59	613.20 ± 3.44	599.24 ± 7.30	622.67 ± 7.05
LVDd (mm)	3.58 ± 0.08	3.51 ± 0.08	3.55 ± 0.04	3.54 ± 0.09
LVDs (mm)	1.99 ± 0.06	2.06 ± 0.05	2.05 ± 0.04	1.97 ± 0.07
FS (%)	44.5 ± 0.87	41.2 ± 0.99	42.2 ± 0.62	44.6 ± 0.91
LVPWth (mm)	0.65 ± 0.11	0.64 ± 0.04	0.81 ± 0.01[A]	0.82 ± 0.01[A]

[A]$P < 0.01$ versus sham. FS, fractional shortening; HR, heart rate; HW/BW, heart-to-body weight ratio; LVDd, LV diameter in end diastole; LVDs, LV diameter in end systole; LVPWth, LV posterior wall thickness in end diastole.

Results

Atrial burst stimulation induces AF in pressure-overloaded hearts. To develop a model of AF associated with LV hypertrophy, we first induced pressure overload in mice by producing transverse aorta constriction (TAC) (25). On day 10, TAC-operated mice showed a significant increase in heart-to-body weight and LV wall thickness with preserved fractional shortening (Table 1). The atrium-to-body weight ratios were increased 36%, from 0.22 ± 0.02 mg/g in sham-operated mice ($n = 5$) to 0.30 ± 0.02 mg/g in TAC-operated mice ($n = 5$; $P < 0.01$), indicating that TAC operation induced hemodynamic overload in both the atrium and ventricle. We recorded ECGs using telemetry at 10 days after the operation, but no episode of spontaneous AF was observed in TAC- or sham-operated mice (Supplemental Figure 1; supplemental material available online with this article; doi:10.1172/JCI39942DS1).

To test the inducibility of AF, we applied programmed electrical stimulation directly to right atrium under Langendorff perfusion at 10 days after the operation. During the period for stabilization prior to stimulation, spontaneous episodes of AF were not observed in TAC- or sham-operated hearts. However, the induction of AF was attainable and reliably reproducible with programmed electrical stimulation of right atrium (Figure 1A). AF was defined as an episode of rapid and chaotic atrial rhythm and irregular ventricular response. AF was induced more frequently in TAC-operated hearts (100%) than in sham-operated hearts (20%) (Figure 1, A–C). In addition, the duration of AF episodes in TAC-operated hearts was significantly longer than that in sham-operated hearts (Figure 1D). We also applied atrial stimulation under Langendorff perfusion at 28 days after TAC operation. However, TAC-operated hearts showed severe LV dysfunction (fractional shortening, 16.6% ± 8.4%) at this time point, and undesirable arrhythmias such as ventricular fibrillation were induced each time after stimulation, which hampered our evaluation of AF arrhythmogenesis. Therefore, atrial burst stimulation under Langendorff perfusion at 10 days after TAC operation represents a valid ex vivo model that permits study of AF substrate, especially in the setting of LV hypertrophy.

Mast cells are accumulated and activated in the atrium of TAC-operated mice. To assess the contribution of mast cells to atrial arrhythmogenicity, we evaluated the contents of mast cells in atrium by staining histological sections with toluidine blue. The number of infiltrating mast cells showed a 2.5-fold increase in TAC-operated mice on day 10, as compared with sham-operated mice (Figure 2A). Avidin conjugated to fluorochrome dyes binds to the negatively charged heparin proteoglycans and identifies the granules of mast cells (20, 26). In the left and right atria of TAC-operated mice, we observed a marked increase of mast cell activation with the presence of extruded avidin-positive granules close to cell surface (Figure 2B). These results suggest that mast cells are accumulated and activated in the atrium of pressure-overloaded hearts.

Stabilization of mast cells by cromolyn attenuates AF in TAC-operated hearts. Accumulation of mast cells in the atrium indicated a causal link between infiltration of these cells and the pathogenesis of AF. To determine the importance of mast cells in this process, we systemically administered the mast cell stabilizer cromolyn (14, 20) to TAC-operated mice. In the atrium at 10 days after TAC operation, the degranulation of mast cells was almost completely inhibited by cromolyn treatment (Figure 2B), although the mast cell contents were not significantly decreased ($P = 0.17$; Figure 2A). Echocardiographic parameters regarding LV hypertrophy and systolic function remained unchanged by cromolyn treatment (Table 1). As revealed by histology, there was no significant difference in the average size of ventricular myocytes between cromolyn- and vehicle-treated mice (Supplemental Figure 2). In addition, the atrium-to-body weight ratios at 10 days after TAC operation were not significantly different between cromolyn- and vehicle-treated mice (0.30 ± 0.02 mg/g vs. 0.28 ± 0.02 mg/g; $P = 0.43$). These results suggest that cromolyn did not affect the hemodynamic workload. However, as compared with vehicle-treated mice, cromolyn-treated mice showed a remarkable reduction in the incidence and duration of AF episodes after atrial burst stimulation under Langendorff perfusion (Figure 3, A–C). To validate and extend our ex vivo findings, we subjected anesthetized mice to rapid transesophageal atrial pacing and simultaneous surface ECG recording at 10 days after the operation. AF could be induced in vivo after atrial burst stimulation in TAC-operated mice, but not in sham-operated mice (Figure 3, D–F). Similarly, cromolyn treatment completely suppressed AF induced by transesophageal atrial pacing in TAC-operated mice (Figure 3, G and H).

Atrial fibrosis is a major feature of structural remodeling that contributes to AF substrate (3, 4). In the atrium of TAC-operated mice, Masson's trichrome staining revealed areas of interstitial fibrosis (Figure 3I), and hydroxyproline assay indicated deposition of collagen (Figure 3J). Mast cell stabilization by cromolyn remarkably attenuated fibrotic changes in the atrium of TAC-operated mice (Figure 3, I and J). These results suggest that stabilization of mast cells prevents atrial structural remodeling and AF inducibility in TAC-operated mice.

Reconstitution with BM cells from mast cell–deficient W/W^v mice attenuates AF in TAC-operated hearts. To further examine the role of mast cells in AF, we utilized mast cell–deficient *WBB6F1-Kit$^{W/W\text{-}v}$* (W/W^v) mice carrying compound heterozygous mutations of *c-kit* (*Kit^W*, null; *Kit$^{W\text{-}v}$*, dominant negative). To circumvent the undesirable effects by altered c-kit signaling in nonhematopoietic cells, we reconstituted C57BL/6 mice with BM cells from W/W^v mice or control *WBB6F1-Kit$^{+/+}$* (+/+) mice. We first confirmed, by tolu-

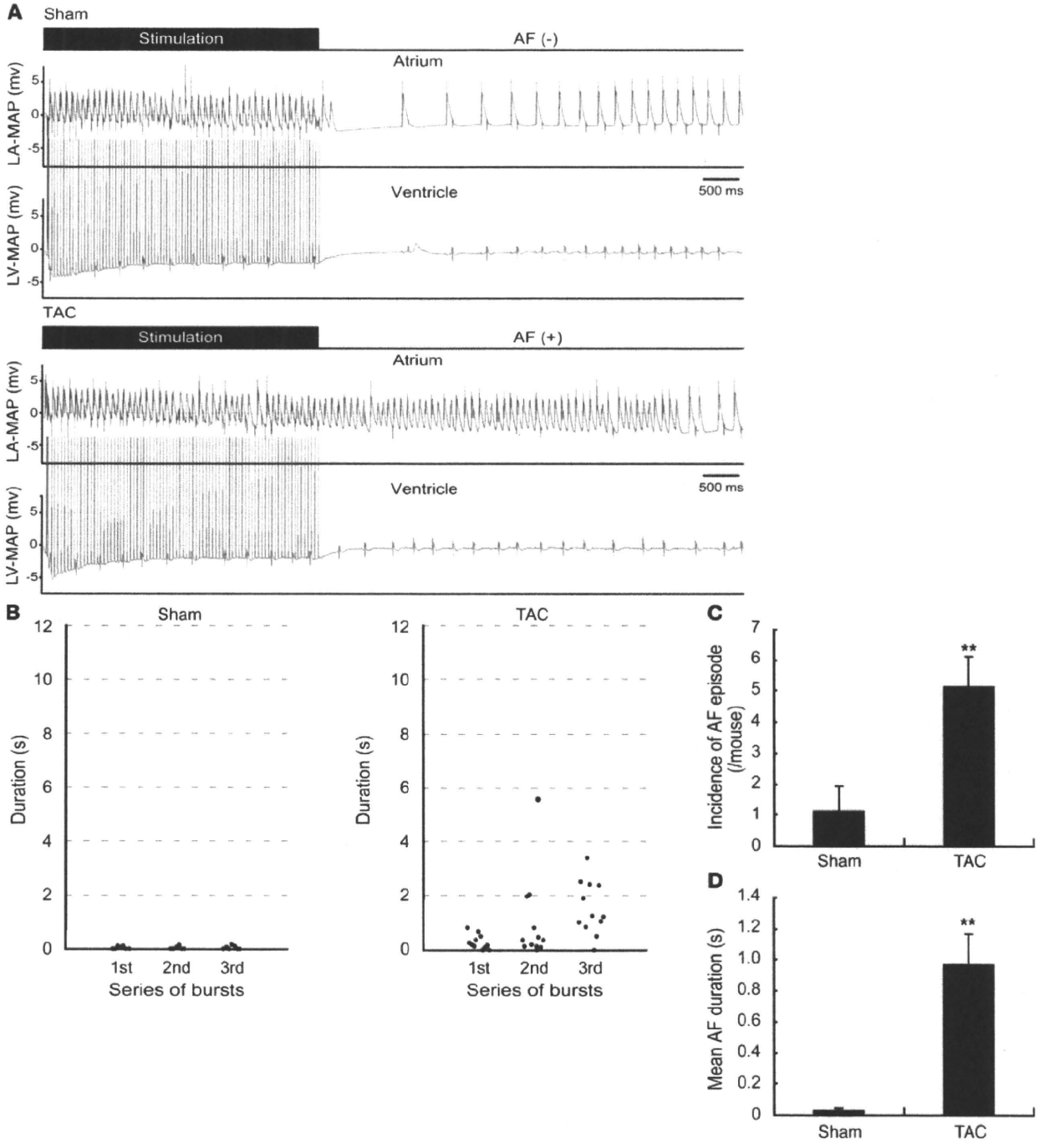

Figure 1

Induction of AF in Langendorff-perfused hearts of mice after TAC operation. (**A**) Termination of the burst of atrial stimulation triggers AF, characterized by rapid and chaotic atrial rhythm and irregular ventricular response, in Langendorff-perfused hearts undergoing TAC operation (lower panels), but not sham operation (upper panels). LA-MAP, monophasic action potential of left atrium; LV-MAP, monophasic action potential of LV. (**B**) AF was triggered in mice undergoing TAC ($n = 5$) or sham ($n = 5$) operation by applying 3 series of bursts with 5-minute intervals. The duration of AF episode occurring after each burst is plotted. (**C**) Incidence of AF episodes during 3 series of bursts in mice undergoing TAC ($n = 5$) or sham ($n = 5$) operation. (**D**) Mean duration of AF episodes during 3 series of bursts in mice undergoing TAC ($n = 5$) or sham ($n = 5$) operation. $^{**}P < 0.01$ versus sham. Data are presented as mean ± SEM.

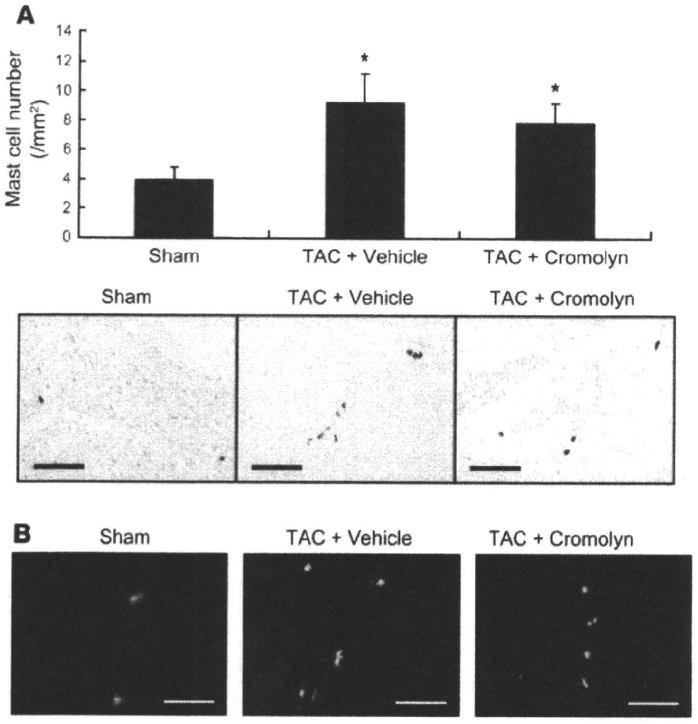

Figure 2

Stabilization of mast cells infiltrating the atrium of TAC-operated mice by cromolyn. (**A**) Representative histological sections with toluidine blue staining for detection of mast cells (purple) in the atrium. Wild-type mice were treated with cromolyn (n = 7) or vehicle (n = 8), and subjected to TAC operation. Mast cell content on day 10 was presented as mean ± SEM. Sham-operated mice were used as control (n = 5). *P < 0.05 versus sham. (**B**) Rhodamine-avidin staining for visualization of mast cell degranulation. Scale bars: 10 μm (**A**); 5 μm (**B**).

idine blue staining, that mast cells were not present in the atrium of mice reconstituted with BM cells from W/W^v mice (W/W^v-BMT mice) after TAC operation, although abundant mast cells infiltrated the atrium of mice reconstituted with BM cells from +/+ mice (+/+-BMT mice) after TAC operation (Figure 4A). Echocardiographic examination revealed that LV hypertrophy after TAC operation did not significantly differ between W/W^v-BMT and +/+-BMT mice, but the fractional shortening in W/W^v-BMT mice was slightly decreased compared with that in +/+-BMT mice (Table 2). In spite of the reduced LV systolic function after TAC operation, the atrium-to-body weight ratios were not significantly different between +/+-BMT mice and W/W^v-BMT mice (0.27 ± 0.02 mg/g vs. 0.31 ± 0.05 mg/g; P = 0.54), and reconstitution with W/W^v BM induced a marked reduction in the incidence and duration of AF episode after atrial burst stimulation compared with +/+ BM reconstitution (Figure 4, B–D). In addition, histological analysis and hydroxyproline assay revealed that atrial fibrosis after TAC operation was attenuated in W/W^v-BMT mice compared with +/+-BMT mice (Figure 4, E and F). These results suggest that deficiency of mast cells prevents atrial structural remodeling and AF inducibility in TAC-operated mice.

BM-derived mast cells cocultured with cardiac myocytes or fibroblasts release PDGF-A to promote fibrinogenesis. In response to a variety of stimuli, mast cells are activated and release numerous bioactive effectors that, either prestored or de novo synthesized, mediate immunoregulatory and proinflammatory effects (11, 24). To delineate mast cell–derived effectors that are involved in the promotion of atrial fibrosis, we examined the gene expressions of fibrosis-related effectors in BM-derived mast cells (BMMCs) after coculture with cardiac myocytes or fibroblasts (Figure 5, A and B, and Supplemental Figure 3). Notably, in quantitative real-time RT-PCR analysis, the mRNA levels of murine *Pdgfa* in BMMCs were prominently elevated after 6 hours coculture with neonatal rat cardiac myocytes or fibroblasts (Figure 5, A and B, and Supplemental Figure 3). In addition, the expression levels of *Pdgfa* were upregulated in the atrium at 10 days after TAC operation, and they were significantly attenuated by reconstitution with W/W^v BM (Figure 5C). These results suggest that mast cells infiltrating the atrium are activated to increase *Pdgfa* gene expression.

Next, we assayed the concentrations of PDGF-AA in medium conditioned by coculture of BMMCs and cardiac fibroblasts. The PDGF-AA concentration showed a more than 3-fold increase after 6 hours coculture, and this increase was remarkably blunted by stabilization of BMMCs with cromolyn during the coculture (Figure 6A). The conditioned medium of coculture promoted cell proliferation of cardiac fibroblasts, and the proliferative effects were abrogated by addition of a neutralizing anti-PDGF α-receptor (anti-PDGFR-α) antibody to the conditioned medium (Figure 6B). Furthermore, the expression of *Col3a1* in cardiac fibroblasts was upregulated after coculture with BMMC, and it was blunted by the treatment with cromolyn or anti-PDGFR-α antibody (Figure 6C). Thus, BMMC-derived PDGF-A can induce cell proliferation and collagen gene expression in cardiac fibroblasts. These results raise a possibility that infiltrating mast cells promote atrial fibrosis and AF inducibility in a PDGF-A–mediated pathway.

Administration of PDGF-AA enhances AF susceptibility in normal hearts. To examine functional significance of atrial *Pdgfa* upregulation in the development of AF substrate, we administered PDGF-AA or vehicle to nonoperated mice and applied atrial burst stimulation. Administration of PDGF-AA for 10 days induced systemic tissue fibrosis, which was particularly prominent in atrium as compared with ventricle (Figure 7A). As a consequence, PDGF-AA–treated hearts showed a significant increase in the incidence and duration of AF episode after atrial burst stimulation under Langendorff perfusion compared with vehicle-treated hearts (Figure 7, B–D). These results suggest that upregulation of *Pdgfa* in atrium can induce atrial fibrosis and enhance AF inducibility in normal hearts.

Neutralization of PDGFR-α attenuates AF in TAC-operated hearts. Next, to examine the role of PDGF-A in the pathogenesis of AF substrate, we inhibited the actions of PDGF-A in TAC-operated hearts by systemic injection of a neutralizing antibody against PDGFR-α (APA5) (27). At 10 days after TAC operation, LV hypertrophy and contraction, as assessed by echocardiography, did not significantly differ between neutralizing antibody–treated mice (TAC-APA5 mice) and control IgG2a-treated mice (TAC-IgG mice) (Table 3). In addition, the atrium-to-body weight ratios were not significantly different between TAC-APA5 and TAC-IgG mice (0.34 ± 0.02 mg/g vs. 0.31 ± 0.03 mg/g; P = 0.44). However, neutralization of PDGFR-α induced a marked reduction

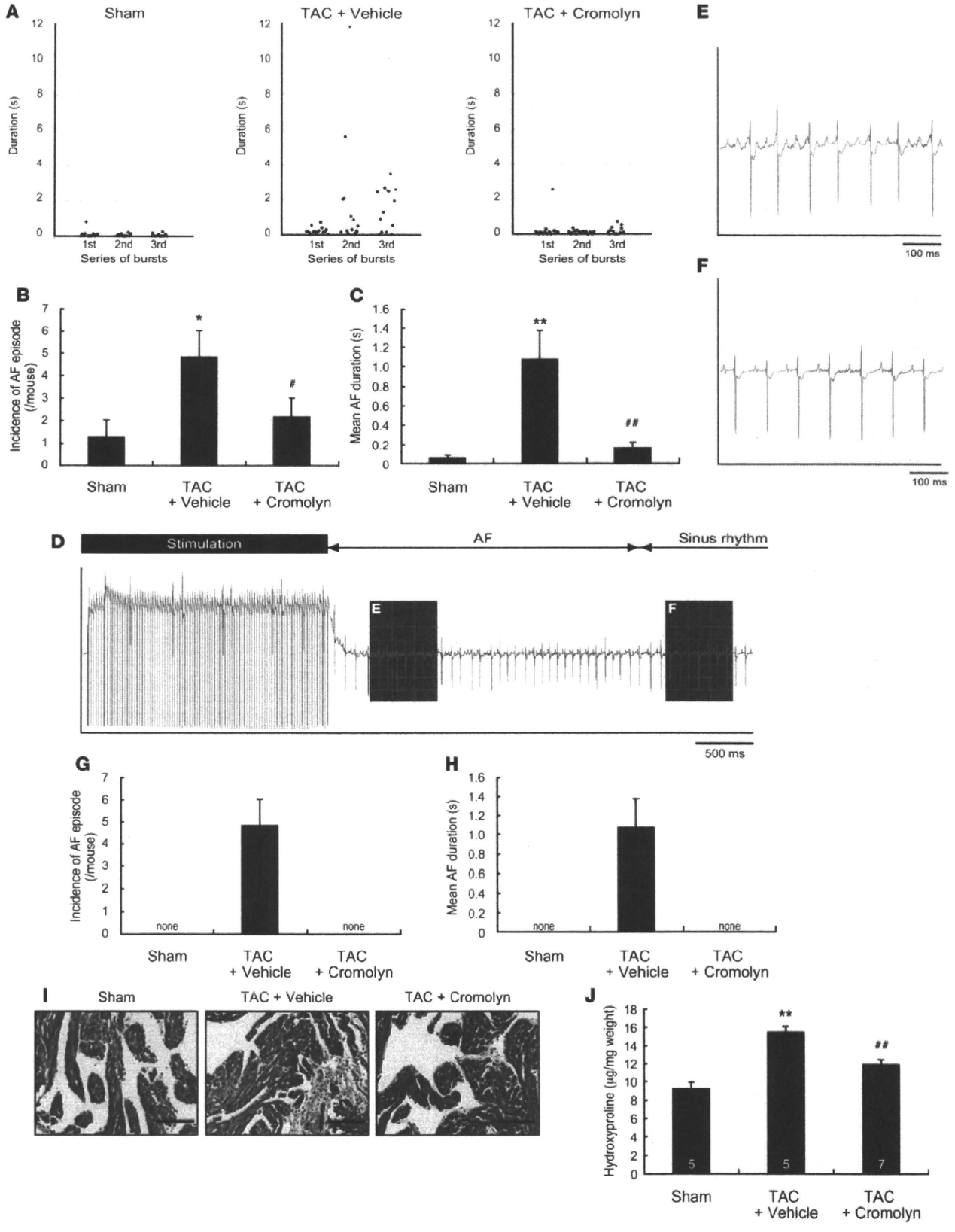
A
Sham
TAC + Vehicle
TAC + Cromolyn
Duration (s)
Series of bursts
1st
2nd
3rd
E
100 ms
F
100 ms
B
Incidence of AF episode (/mouse)
C
Mean AF duration (s)
Sham
TAC + Vehicle
TAC + Cromolyn
D
Stimulation
AF
Sinus rhythm
500 ms
G
H
none
I
J
Hydroxyproline (μg/mg weight)
5
5
7

Figure 3
Attenuation of AF and atrial fibrosis by mast cell stabilization by cromolyn. (**A**) Scatter plot of the duration of AF episodes occurring during 3 series of bursts in Langendorff-perfused hearts (n = 10). (**B**) Incidence of AF episodes during 3 series of bursts under Langendorff perfusion (n = 10). *P < 0.05 versus sham; #P < 0.05 versus TAC treated with vehicle. (**C**) Mean duration of AF episodes during 3 series of bursts under Langendorff perfusion (n = 10). **P < 0.01 versus sham; ##P < 0.01 versus TAC treated with vehicle. (**D**) Representative surface ECG in lead-II deflection of AF induced by termination of the burst of transesophageal atrial pacing in TAC-operated mice. (**E**) High-magnification view of the section delineated by shaded box in **D**, showing AF with chaotic atrial rhythm and irregular ventricular response. (**F**) High-magnification view of the section delineated by shaded box in **D**. AF was spontaneously converted to sinus rhythm. (**G**) Incidence of AF episodes during 3 series of transesophageal bursts (n = 6). (**H**) Mean duration of AF episodes during 3 series of transesophageal bursts (n = 6). (**I**) Representative histological sections with Masson's trichrome staining for visualization of atrial fibrosis (blue staining). Scale bars: 20 μm. (**J**) Hydroxyproline content in the atrium. Number of mice for each experiment is indicated in the bars. **P < 0.01 versus sham; ##P < 0.01 versus TAC treated with vehicle. Data are presented as mean ± SEM.

in the incidence and duration of AF episode both after atrial burst stimulation under Langendorff perfusion (Figure 8, A–C) and after transesophageal atrial pacing in vivo (Figure 8, D and E). In addition, histological analysis and hydroxyproline assay revealed that atrial fibrosis was attenuated in TAC-APA5 mice compared with TAC-IgG mice (Figure 8, F and G). Thus, the effects of cromolyn treatment or BM reconstitution from W/W^v mice on AF substrate were reproduced by neutralization of PDGFR-α in TAC-operated hearts. These results suggest that PDGF-A mediates the deleterious effects of mast cells to promote atrial fibrosis and AF inducibility.

Discussion

Clinical and experimental studies have suggested that inflammation underlies a susceptible AF substrate, which is characterized by interstitial fibrosis in atrium. Our present study demonstrated a hitherto unknown role of mast cells in the development of a susceptible AF substrate. Mast cells were accumulated and activated in the atrium of pressure-overloaded mice, and pharmacological stabilization or genetic depletion of mast cells prevented atrial structural remodeling and reduced the incidence and duration of AF following atrial burst stimulation. Notably, infiltrating mast cells induced upregulation of PDGF-A in the atrium, and neutral-

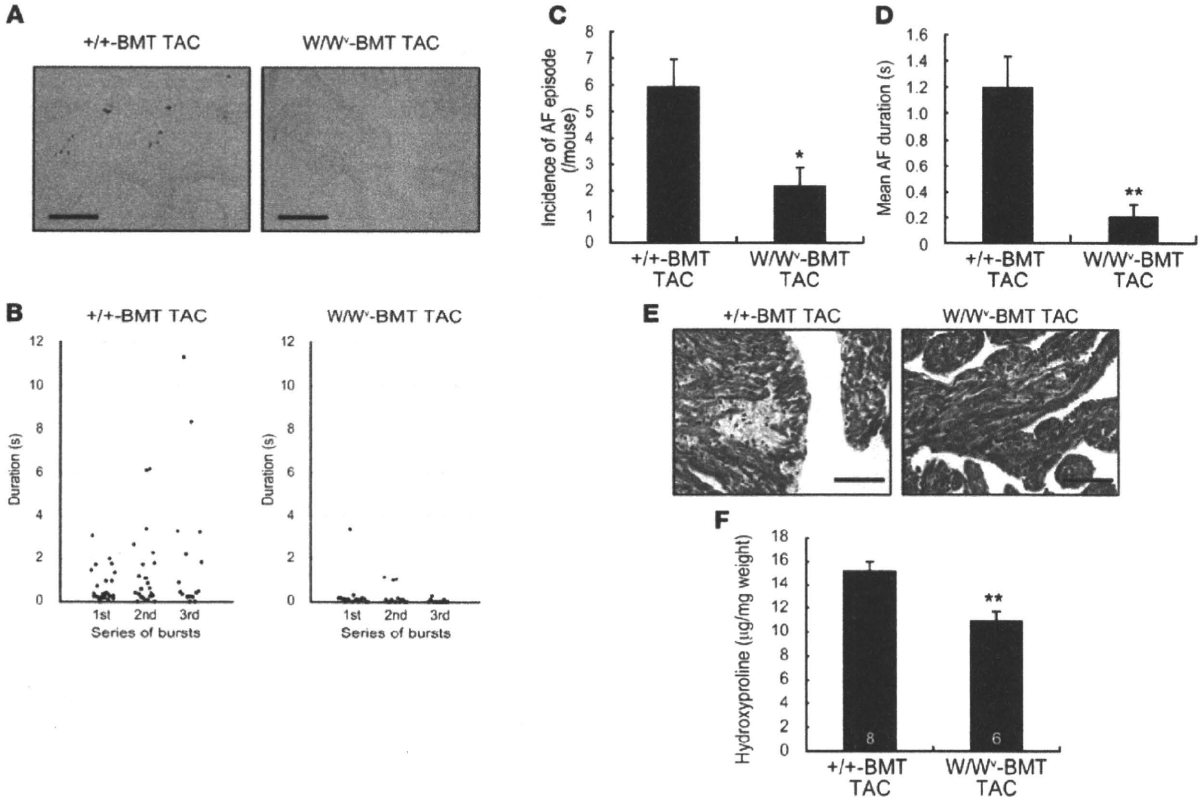

Figure 4
Attenuation of atrial fibrosis and AF by reconstitution with BM cells from W/W^v mice. (**A**) Representative histological sections with toluidine blue staining. Mast cells were not present in the atrium of TAC-operated W/W^v-BMT mice. (**B**) Scatter plot of the duration of AF episodes occurring during 3 series of bursts in TAC-operated W/W^v-BMT mice (n = 11) or +/+-BMT mice (n = 11). (**C**) Incidence of AF episodes during 3 series of bursts (n = 11). *P < 0.05 versus +/+-BMT mice. (**D**) Mean duration of AF episodes during 3 series of bursts (n = 11). **P < 0.01 versus +/+-BMT mice. (**E**) Representative histological sections with Masson's trichrome staining for visualization of atrial fibrosis (blue staining). (**F**) Hydroxyproline content in the atrium. Number of mice for each experiment is indicated in the bars. Scale bars: 10 μm (**A**); 20 μm (**E**). Data are presented as mean ± SEM.

Table 2
Echocardiographic measurements in TAC- or sham-operated W/W^v-BMT or +/+-BMT mice

	Sham		TAC	
	+/+-BMT	W/W^v-BMT	+/+-BMT	W/W^v-BMT
Number	9	9	9	9
HW/BW (mg/g)	4.42 ± 0.14	4.42 ± 0.13	5.51 ± 0.10^A	5.34 ± 0.16^A
HR (bpm)	636.63 ± 7.78	629.22 ± 2.89	613.20 ± 9.34	612.33 ± 6.78
LVDd (mm)	3.68 ± 0.05	3.61 ± 0.07	3.55 ± 0.07	3.69 ± 0.07
LVDs (mm)	2.30 ± 0.05	2.15 ± 0.05	2.05 ± 0.04^A	2.28 ± 0.08^B
FS (%)	39.3 ± 0.93	40.4 ± 0.44	41.6 ± 0.26^C	38.96 ± 1.32^D
LVPWth (mm)	0.61 ± 0.01	0.58 ± 0.01	0.68 ± 0.01^A	0.66 ± 0.02^A

$^AP < 0.01$ versus sham. $^BP < 0.01$ versus TAC-operated +/+-BMT. $^CP < 0.05$ versus sham. $^DP < 0.05$ versus TAC-operated ++-BMT.

ization of PDGFR-α prevented atrial fibrosis and AF inducibility, indicating a pivotal role of PDGF-A in mast cell–triggered AF. It has been reported that atrial arrhythmias and fibrillation occur with extremely low frequency in mice because the atrium is too small in size to maintain multiple-circuit reentry (28). Indeed, we did not detect any spontaneous episode of AF in TAC-operated mice by ECG telemetry (Supplemental Figure 1), but atrial burst stimulation reproducibly induced AF either in ex vivo or in vivo hearts subjected to pressure overload (Figures 1 and 3). Although the duration of AF was limited in length as compared with that in large animal models, a mouse model is powerful for dissection of the causal relationship between arrhythmogenesis and genetic or cellular factors. Although transesophageal pacing in vivo is minimally invasive for atrial stimulation, the incidence of AF was relatively low even in TAC-operated mice (50%), and an anesthetic agent might influence the inducibility and duration of AF in an in vivo model (28). In this regard, atrial stimulation under Langendorff perfusion is a suitable and reliable model of AF that provides mechanistic and therapeutic insights into development of an AF substrate in the setting of hemodynamic overload.

Besides orchestrating allergic and immune responses, mast cells participate in the inflammatory process that underlies the development of cardiovascular diseases (11). Insomuch as the number of infiltrating mast cells at the affected lesions is significantly increased but yet relatively low, it has been difficult to characterize the relevance of these cells to the pathogenesis of a disease. However, mice genetically deficient for mast cells allow assessment of

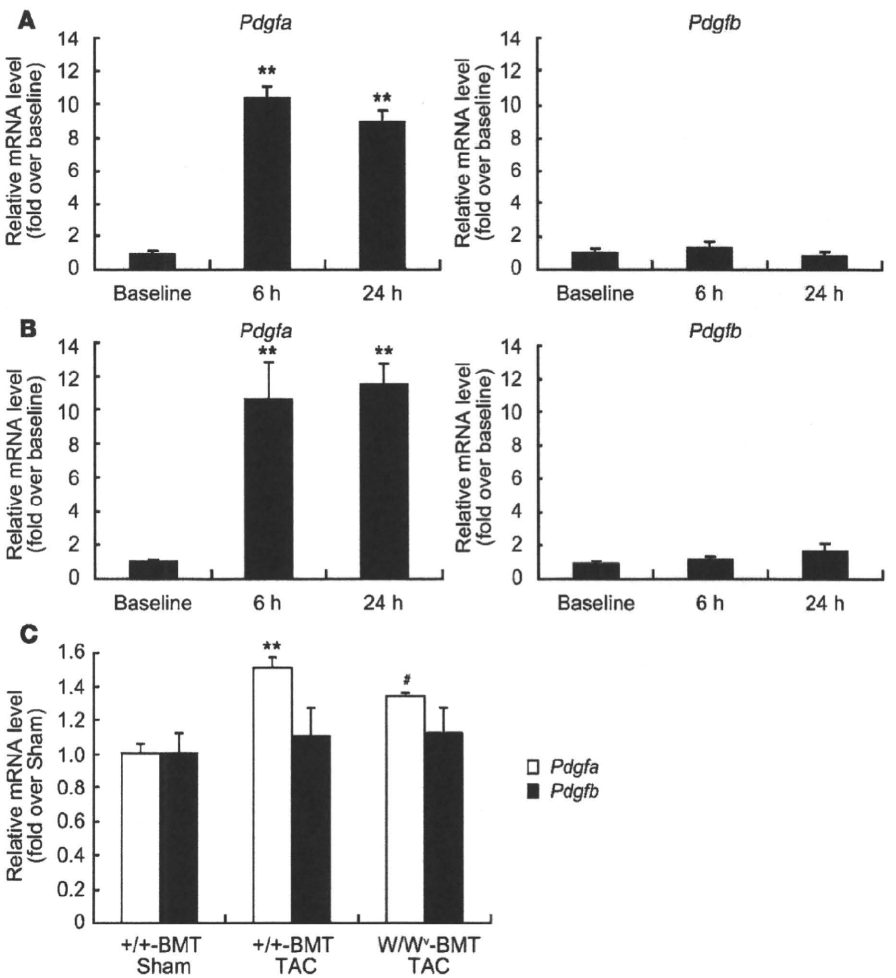

Figure 5
Mast cell–mediated upregulation of *Pdgfa* expression in the atrium of TAC-operated hearts. (**A**) mRNA expression of *Pdgfa* and *Pdgfb* in BMMCs at baseline, 6 hours, and 24 hours after coculture with cardiac myocytes. Experiments were repeated 4 times in triplicate. $^{**}P < 0.01$ versus baseline. (**B**) mRNA expressions of *Pdgfa* and *Pdgfb* in BMMCs at baseline, 6 hours, and 24 hours after coculture with cardiac fibroblasts. Experiments were repeated 5 times in triplicate. $^{**}P < 0.01$ versus baseline. (**C**) mRNA expressions of *Pdgfa* and *Pdgfb* in the atrium of sham-operated mice ($n = 8$), TAC-operated W/W^v-BMT mice (W/W^v-BMT TAC, $n = 7$), or +/+ mice (+/+-BMT TAC, $n = 6$). $^{**}P < 0.01$ versus sham; $^{\#}P < 0.05$ versus +/+-BMT TAC. Data are presented as mean ± SEM.

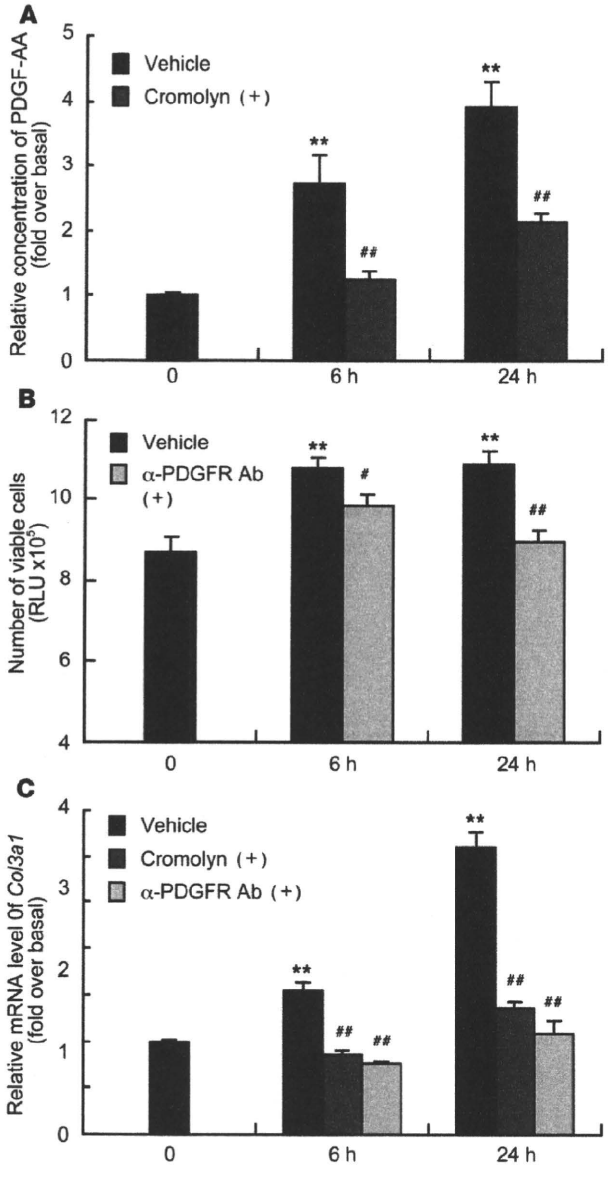

Figure 6

BMMC-derived PDGF-A can induce cell proliferation and collagen gene expression in cardiac fibroblasts. (**A**) ELISA analysis of PDGF-AA content in conditioned medium at baseline, 6 hours, and 24 hours after coculture of BMMCs and cardiac fibroblasts with or without cromolyn (10 μM). Experiments were repeated 5 times in triplicate. $^{**}P < 0.01$ versus baseline; $^{\#\#}P < 0.01$ versus vehicle. (**B**) Number of viable cardiac fibroblasts at baseline, 6 hours, and 24 hours after culture in medium-conditioned coculture of BMMCs and cardiac fibroblasts with or without a neutralizing anti–PDGFR-α antibody (2 μg/ml), as assessed by relative amount of ATP. Experiments were repeated 4 times in triplicate. $^{**}P < 0.01$ versus baseline; $^{\#}P < 0.05$; $^{\#\#}P < 0.01$ versus vehicle. (**C**) mRNA expressions of *Col3a1* in cardiac fibroblasts cocultured with BMMCs with or without cromolyn (10 μM) or a neutralizing anti–PDGFR-α antibody (2 μg/ml) at baseline, 6 hours, and 24 hours. Experiments were repeated 4 times in triplicate. $^{**}P < 0.01$ versus baseline; $^{\#\#}P < 0.01$ versus vehicle. Data are presented as mean ± SEM.

the contributions of mast cell function to biological responses in vivo (11). In this study, we utilized *c-kit* mutant W/W^v mice that are profoundly mast cell deficient (29) and virtually lack melanocytes and interstitial Cajal cells (30). According to a recent paper, *c-kit* is also expressed in cardiac stem cells and cardiac myocytes and plays a regulatory role in the differentiation of these cells (31). Thus, to avoid the effects of *c-kit* mutation on cardiac myocytes, we reconstituted C57BL/6 mice with BM from W/W^v mice. BM reconstitution from W/W^v mice influenced contractile function, which might be related to hematological abnormalities such as macrocytic anemia (32). In spite of the hemodynamic burden, atrial structural remodeling and AF susceptibility were blunted by BM reconstitution from W/W^v mice, which underpinned the functional importance of mast cells in the AF pathogenesis of pressure-overloaded hearts.

Mast cells exist in the heart under physiological conditions (13), and mast cell density in heart tissues of patients with cardiomyopathy is elevated, as compared with normal hearts (33). Mast cells are long lived in the tissue and can reenter cell cycle and proliferate locally (34). A variety of chemokines have been identified that induce local recruitment of mast cells, such as SCF, monocyte chemoattraction protein-1 (MCP-1), nerve growth factor (NGF), and RANTES (24). In addition, interactions between mast cells and connective tissue matrix components have profound influences on the distribution of mast cells in tissues (35–37). Although the most important trigger for mast cell activation is antigen- and IgE-dependent aggregation of IgE receptor (FcεRI), mast cells can be activated by various factors, such as cytokines, growth factors, and hormones (11, 12, 24). In our study, coculture with cardiac myocytes or fibroblasts per se promoted gene expression of some cytokines in BMMCs. We postulate that a certain paracrine- or cell-to-cell contact–dependent signaling may trigger mast cell activation in hearts. Further investigation will be required to delineate the precise mechanisms of how cardiac mast cells are accumulated and activated in stressed hearts.

Mast cells secrete diverse chemical mediators, cytokines, and growth factors upon exposure to a stimulus. This process involves release of the mediators prestored in the granules (degranulation) and de novo synthesis of mediators. Differential synthesis of mast cell mediators is dependent on the particular mechanism of activation and the strength of the stimulus and is crucially involved in the inflammatory process (12, 24). We identified PDGF-A as a crucial molecule that mediates mast cell–induced atrial fibrosis. Among the fibrogenic mediators, upregulation of *Pdgfa* in BMMCs was pronounced after coculture either with cardiac myocytes or fibroblasts. In our coculture experiments, BMMC-derived PDGF-A accelerated proliferation of cardiac fibroblasts and stimulated synthesis of type III collagen in cardiac fibroblasts. PDGF-A dimeric isoform (PDGF-AA) selectively binds to PDGFR-α (38), and PDGF-AA infusion exerted potent fibrogenic effects, particularly on atrium (Figure 7A), consistent with a previous paper demonstrating that atrial fibroblasts showed higher reactivity to PDGF than ventricular fibroblasts (39). Importantly, the mRNA levels of *Pdgfa* in atrium were significantly increased after TAC operation, which was blunted by depletion of mast cells by BM reconstitution from W/W^v mice. PDGF-A production in atrium is critically relevant to the AF pathogenesis of pressure-overloaded hearts because neutralization of PDGFR-α prevented atrial fibrosis and AF. Collectively, our results suggest that atrial mast cells induce upregulation

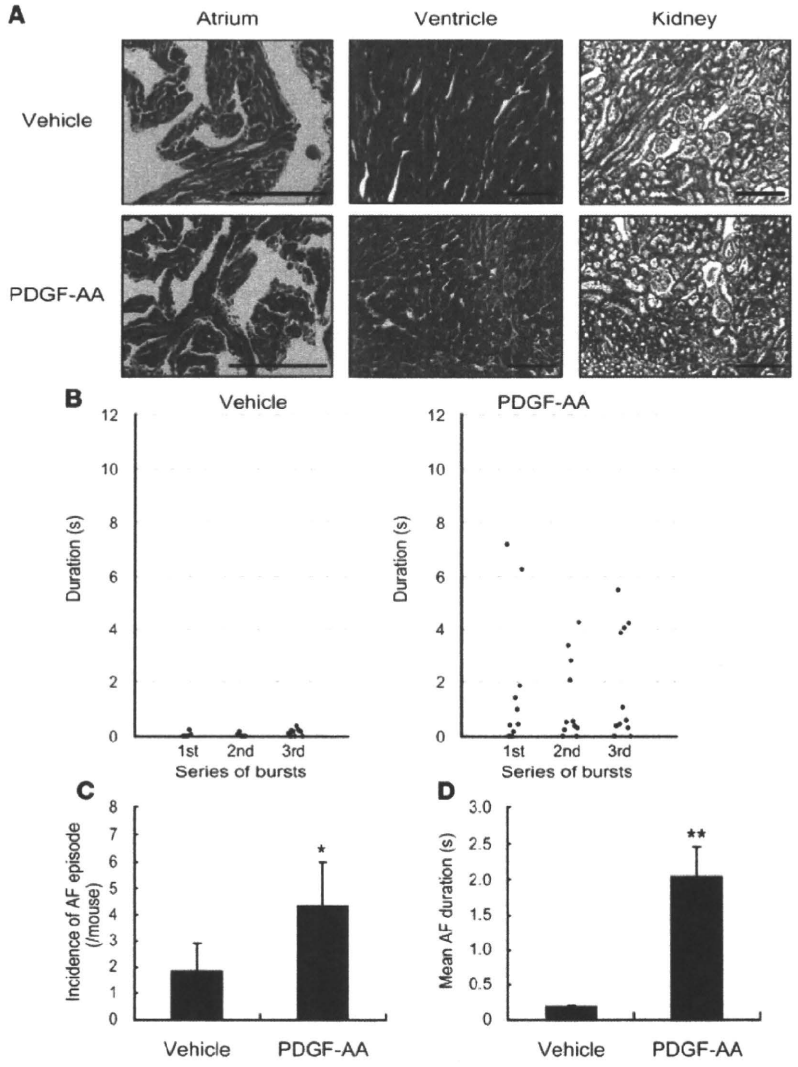

Figure 7
Systemic administration of PDGF-AA induces atrial fibrosis and enhances AF susceptibility in Langendorff-perfused hearts. (**A**) Representative histological sections with Masson's trichrome staining for visualization of fibrosis (blue staining) in the atrium, ventricle, and kidney of mice administered PDGF-AA or vehicle. Scale bars: 20 μm. (**B**) Scatter plot of the duration of AF episodes occurring during 3 series of bursts in mice administered PDGF-AA ($n = 6$) or vehicle ($n = 6$). Duration of AF episodes occurring after each burst are plotted. (**C**) Incidence of AF episodes during 3 series of bursts in mice administered PDGF-AA ($n = 6$) or vehicle ($n = 6$). (**D**) Mean duration of AF episodes during 3 series of bursts in mice administered PDGF-AA ($n = 6$) or vehicle ($n = 6$). Data are presented as mean ± SEM. $^*P < 0.05$ versus vehicle; $^{**}P < 0.01$ versus vehicle.

of *Pdgfa*, leading to progression of a susceptible AF substrate in pressure-overloaded hearts. At present, it remains uncertain whether atrial mast cells are the sole source of PDGF-A. Indeed, mast cell activation can influence the function of many different cell types (12, 24), and especially, macrophages may serve as a source of PDGF-A (38). Further studies using an intricate genetic model to delete *Pdgfa* specifically in mast cells will be required to dissect the importance of mast cell–derived PDGF-A in the pathogenesis of AF.

Several clinical studies have proved the efficacy of pharmacological inhibition of the renin-angiotensin system in the prevention of atrial fibrosis and promotion of AF (40). The therapeutic approach to attenuating or reversing the AF substrate is appealing. Our study highlighted the pathogenic role of mast cells in promoting the AF substrate in pressure-overloaded hearts. Of course, this observation must be further investigated in future studies using large animal models for testing applicability to clinical conditions because variability among species and experimental models may give rise to differences in anatomical and electrophysiological parameters (41). As a starting point for investigations, we propose that the mast cell–PDGF-A axis will be a promising therapeutic target for the upstream prevention of AF in stressed hearts.

Methods

Mice, TAC operation, and echocardiography. All of the experimental protocols were approved by the Institutional Animal Care and Use Committee of Chiba University. C57BL/6 mice, mast cell–deficient W/W^v mice, and congenic +/+ littermates were purchased from Japan SLC. For TAC operation, 10-week-old male mice were anesthetized by i.p. injection of pentobarbital, and respiration was artificially controlled with a tidal volume of 0.2 ml and a respiratory rate of 110 breaths/min. The transverse aorta was constricted with 7-0 nylon strings by ligating the aorta with splinting a blunted 27-gauge needle, which was removed after the ligation. After aortic constriction, the chest was closed and mice were allowed to recover from anesthesia. We confirmed that the magnitude of initial pressure elevation after aortic banding was identical in all groups of mice. The surgeon had no information about the mice used in this study. For evaluation of cardiac dimensions and contractility, transthoracic echocardiography was performed on conscious mice with the Vevo 770 Imaging System using a 25-MHz linear probe (Visual Sonics).

Table 3
Echocardiographic measurements in TAC-APA5 or TAC-IgG mice

	TAC-IgG	TAC-APA5
Number	10	10
HW/BW (mg/g)	5.71 ± 0.18	5.67 ± 0.16
HR (bpm)	633.30 ± 16.06	657.00 ± 11.91
LVDd (mm)	3.54 ± 0.09	3.59 ± 0.08
LVDs (mm)	2.07 ± 0.09	2.01 ± 0.09
FS (%)	41.7 ± 1.48	44.2 ± 1.51
LVPWth (mm)	0.84 ± 0.01	0.81 ± 0.01

Mast cell stabilization and BM reconstitution. For stabilization of mast cells, cromolyn (50 mg/kg/day; Sigma-Aldrich) or vehicle was administrated daily to mice by i.p. injection (14) for the duration of the experiment (10 days after TAC operation). For BM reconstitution, BM cell suspensions were harvested by flushing the femurs and tibias of 8-week-old W/W^v or +/+ mice. The 5-week-old C57BL/6 mice were preconditioned with total body irradiation (9.5 Gy) 6 hours before transplantation. BM cell suspensions (1.0×10^7 cells per mouse) were transfused via the tail vein to the preconditioned recipient mice. The recipient mice were subjected to BM reconstitution for 6 weeks and were subjected to TAC operation.

Induction of AF in ex vivo and in vivo hearts. For induction of AF in ex vivo hearts, hearts were rapidly excised after i.p. injection of heparin (0.5 U/g) and urethane (2 mg/g) and immediately mounted onto a Langendorff perfusion apparatus (42). The hearts were perfused with a nonrecirculating Krebs-Henseleit buffer (119 mM NaCl, 4.8 mM KCl, 1.2 mM KH_2PO_4, 1.2 mM $MgSO_4$, 2.5 mM $CaCl_2$, 10 mM glucose, and 24.9 mM $NaHCO_3$), which was equilibrated with 5% CO_2/95% O_2 at 37°C. All isolated hearts were stabilized for 5 minutes by perfusion at constant flow (3.0 ± 0.2 ml/min) before programmed electrical stimulation. The whole system temperature was kept at 37°C. Two chlorinated silver wires were placed on the base of the heart as indifferent and common ground electrodes. A pair of recording electrodes were placed on the apex and anterior wall of the heart to record ventricular electrograms. Bipolar stimulating electrodes were pressed against the right atrium surface, and bipolar recording electrodes were placed on the left atrium surface to record atrial electrograms.

For induction of AF in in vivo hearts, mice were anesthetized with i.p. injection of pentobarbital and supported by artificial ventilation. The body temperature of mice was monitored and kept at 37°C using a heating pad during the experiments. A 2-French catheter electrode (Japan Lifeline) was placed at the esophageal position dorsal to the left atrium. A surface ECG was simultaneously recorded using electrodes in a lead-II configuration.

Inducibility of AF was tested by applying a 2-second burst using the automated stimulator. The first 2-second burst had a cycle length (CL) of 40 ms, decreasing in each successive burst with a 2-microsecond decrement down to a CL of 20 ms. A series of bursts was repeated 3 times after stabilization for 5 minutes. AF duration was defined as the interval between the rapid irregular atrial rhythm triggered after the bursts and the onset of first normal sinus beat.

Histological analysis. Hearts were excised and immediately fixed in 10% neutralized formalin, and they were then embedded in paraffin. Serial sections of atrium at 5 μm were stained with Masson's trichrome for evaluation of fibrosis. We determined mast cell number and morphology with toluidine blue staining (0.1%; Sigma-Aldrich) and rhodamine-avidin staining (1:100; Vector Laboratories) (20, 26). Specificity of mast cell detection was confirmed by staining sections of W/W^v and +/+ mice at the same dilution of the reagent. The total number of mast cells was counted manually and blindly in 3 microscopic sections from each mouse, and the total area was determined using computer-assisted image analysis (ImageJ; http://rsbweb.nih.gov/ij/).

Hydroxyproline assay. We evaluated collagen content in the atrium by quantification of hydroxyproline, as described previously (43). In brief, the atrium was weighed and then hydrolyzed in 6 N HCl at 100°C overnight. Hydrolyzed tissue was neutralized with NaOH, vacuum dried at 50°C, and resuspended in 1 ml of 5 mM HCl. An aliquot of 20 μl hydrolyzed tissue was added to 180 μl of H_2O in a glass tube. Thereafter, we mixed 100 μl of chloramine-T solution (0.14 g chloramine-T, Sigma-Aldrich; 2 ml H_2O, 8 ml hydroxyproline assay buffer) with the diluted hydrolyzed tissue solution. The ingredients of hydroxyproline assay buffer were as follows: 11.4 g sodium acetate anhydrous (Sigma-Aldrich), 7.5 g trisodium citrate dihydrate (Sigma-Aldrich), 40 ml H_2O (pH adjusted to 6.0), and 77 ml isopropanol, bringing the final volume to 200 ml with H_2O. After incubation for 10 minutes at room temperature, 1.25 ml Ehrlich's reagent (6.0 g p-dimethylaminobenzaldehyde [Sigma-Aldrich], 18 ml 60% perchlorate [Fluka], 78 ml isopropanol) was added and mixed. The samples were incubated at 55°C for 20–25 minutes, and the sample absorbance was read at 558 nm. We used *trans*-4-hydroxy-L-proline (Sigma-Aldrich) (ranging from 0 to 4 mg) to draw the standard curve.

Coculture of BMMCs with cardiac myocytes or fibroblasts. The BM cells were harvested from C57BL/6 mice and cultured for 5 weeks in RPMI 1640 medium (GIBCO; Invitrogen) supplemented with 10% FBS (Equitech-Bio), 0.1 mM MEM Non-Essential Amino Acids Solution (GIBCO; Invitrogen), 4 mM L-glutamine, 25 mM HEPES, 1 mM sodium pyruvate, 50 μM β-mercaptoethanol, 100 U/ml penicillin, 100 μg/ml streptomycin, and 30 ng/ml of recombinant murine IL-3 (PeproTech GmbH) at 37°C in 5% CO_2 (44). By 5 weeks in culture, mast cells were enriched to more than 95%, as assessed by the presence of metachromatic granules in toluidine blue–stained cells and by cell-surface expression of FcεRI (Upstate) using flow cytometric analysis. The cardiac myocytes and fibroblasts were prepared from hearts of 1-day-old Wistar rats, as described previously (45). Dissociated cells were preplated onto 10-cm culture dishes for 30 minutes, which permitted preferential attachment of fibroblasts to the bottom of the dish. Nonadherent cardiac myocytes (3.5×10^5 cells/3.5-cm dish) or adherent fibroblasts (2.0×10^6 cells/3.5-cm dish) were plated on 3.5-cm dishes and cultured for 24 hours in medium (DMEM [GIBCO; Invitrogen], supplemented with 10% FBS, 100 U/ml penicillin, and 100 μg/ml streptomycin). The cells were starved under a serum-free condition for 24 hours before initiation of the coculture. BMMCs (5.0×10^6 cells/3.5-cm dish) were placed onto layers of cardiac myocytes or fibroblasts and were continuously cocultured in DMEM without supplementation with FBS. For stabilization of BMMCs in vitro, BMMCs were pretreated with 10^{-5} M cromolyn (Sigma-Aldrich) for 30 minutes before initiation of coculture, and cromolyn treatment was continued throughout the coculture.

Real-time RT-PCR analysis. Total RNA was extracted by using RNeasy Kit (QIAGEN), and single-stranded cDNA was transcribed by using QuantiTect Reverse Transcription Kit (QIAGEN) according to the manufacturer's protocol. We conducted quantitative real-time PCR analysis with the Universal ProbeLibrary Assays (Roche Applied Science) according to the manufacturer's instructions. Amplification conditions were as follows: initial denaturation for 10 minutes at 95°C followed by 45 cycles of 10 seconds at 95°C and 25 seconds at 60°C. Individual PCR products were analyzed by melting-point analysis. The expression level of a gene was normalized relative to that of *Gapdh* by using a comparative Ct method. The primer sequences and universal probe numbers were designed with the ProbeFinder software as follows: *Pdgfa*, 5′-GTGCGACCTCCAACCTGA-3′ and 5′-GGCTCATCTCACCTCACATCT-3′, no. 52; *Pdgfb*, 5′-CGGCCTGTGACTAGAAGTCC-3′ and 5′-GAGCTTGAGGCGTCTTGG-3′, no. 32; *Col3a1*, 5′-TCCCCTG-

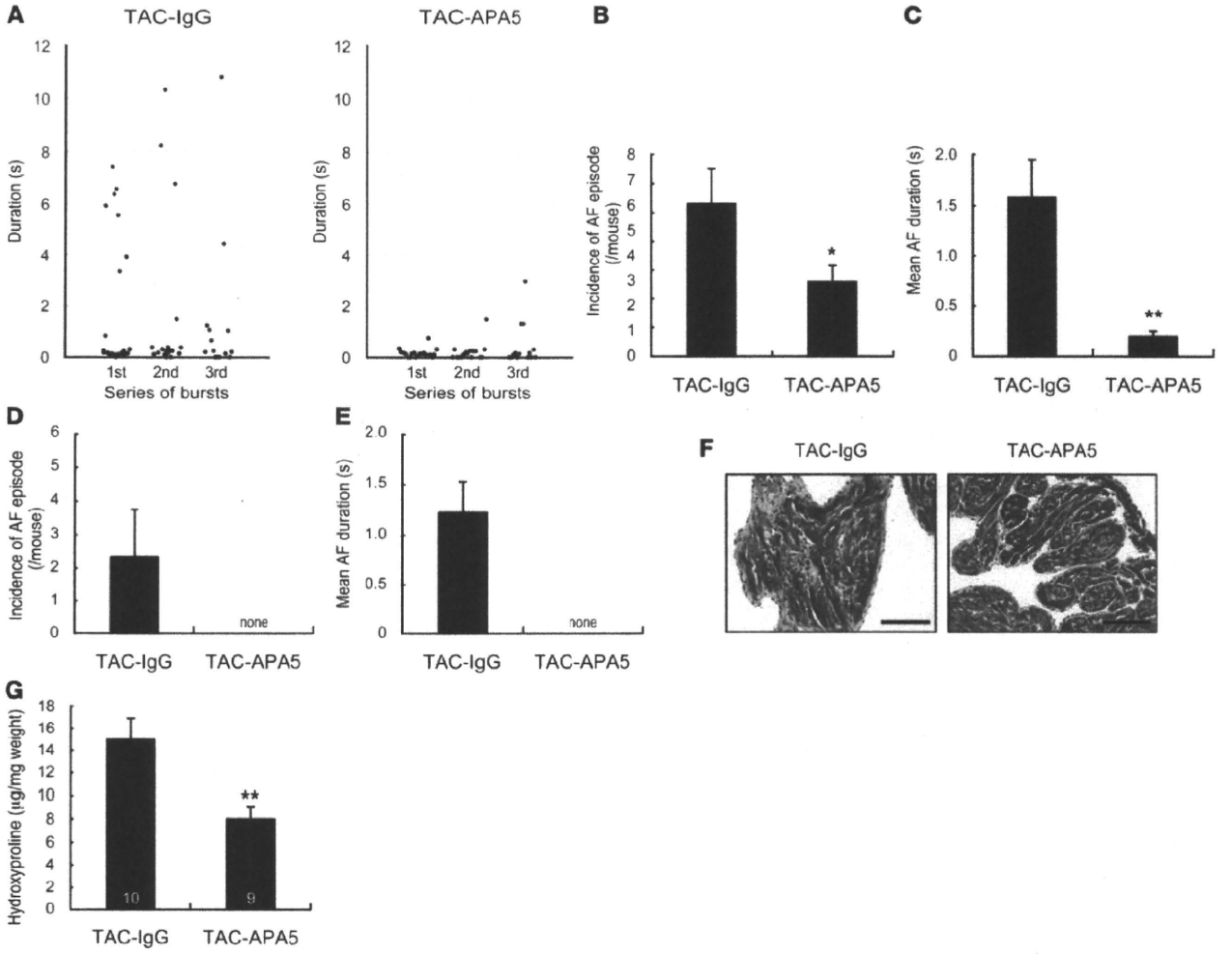

Figure 8

Attenuation of atrial fibrosis and AF by neutralization of PDGFR-α. (**A**) Scatter plot of duration of AF episodes occurring during 3 series of bursts under Langendorff perfusion in TAC-APA5 ($n = 9$) or TAC-IgG mice ($n = 9$). (**B**) Incidence of AF episodes during 3 series of bursts under Langendorff perfusion ($n = 9$). $^*P < 0.05$ versus control IgG. (**C**) Mean duration of AF episodes during 3 series of bursts under Langendorff perfusion ($n = 9$). $^{**}P < 0.01$ versus control IgG. (**D**) Incidence of AF episodes during 3 series of transesophageal bursts ($n = 6$). (**E**) Mean duration of AF episodes during 3 series of transesophageal bursts ($n = 6$). (**F**) Representative histological sections with Masson's trichrome staining for visualization of atrial fibrosis (blue staining). Scale bars: 20 μm. (**G**) Hydroxyproline content in the atrium ($n = 9$). Number of mice for each experiment is indicated in the bars. $^{**}P < 0.01$ versus control IgG. Data are presented as mean ± SEM.

GAATCTGTGAATC-3′ and 5′-TGAGTCGAATTGGGGAGAAT-3′, no. 49; mouse *Gapdh*, 5′-TGTCCGTCGTGGATCTGAC-3′ and 5′-CCTGCTTCAC-CACCTTCTTG-3′, no. 80; rat *Gapdh*, 5′-TGGGAAGCTGGTCATCAAC-3′ and 5′-GCATCACCCCATTTGATGTT-3′, no. 9.

ELISA of PDGF-AA. The concentrations of PDGF-AA in the conditioned medium were assayed by using Human/Mouse PDGF-AA Quantikine ELISA Kit (R&D Systems) according to the manufacturer's protocol.

Cell proliferation assay. Cardiac fibroblasts (2×10^4 cells/well) were plated on a 48-well plate and were cultured for 24 hours in medium (DMEM supplemented with 10% FBS, 100 U/ml penicillin, and 100 μg/ml streptomycin) at 37°C in 5% CO_2. After 24 hours of starvation under serum-free conditions, we replaced the medium with that conditioned by coculture of BMMCs and cardiac fibroblasts. After 24 hours of culture, cells were harvested, and subjected to semiquantification of the viable cell numbers that are proportional to the amount of ATP by using CellTiter-Glo Luminescent Cell Viability Assay Kit (Promega).

Systemic administration of PDGF-AA. Mini-osmotic pumps (model 2002; Alzet) were subcutaneously implanted in 10-week-old male mice to deliver recombinant murine PDGF-AA (0.2 μg/day; PeproTech) or vehicle. At 10 days after implantation, mice were sacrificed for analysis.

Inhibition of PDGF-A by a neutralizing anti–PDGFR-α antibody. To antagonize the effects of BMMC-derived PDGF-A in vitro, we pretreated BMMCs with 2 μg/ml of clone APA5 (200 μg/day) (27) or control IgG2a (eBioscience) for 30 minutes before initiation of coculture and continued the treatment throughout the coculture. To inhibit the effects of PDGF-A in vivo, we administered anti-PDGFR-α antibody (200 μg/day) (27) or control IgG2a by i.p. injection to mice for the duration of the experiment (10 days after TAC operation). APA5, a rat monoclonal anti-mouse PDGFR-α antibody (IgG2a), was described previously (46).

Statistics. All data are presented as means ± SEM. Two-group comparison was analyzed by unpaired 2-tailed Student's *t* test, and multiple-group comparison was performed by 1-way ANOVA followed by the Fisher's pro-

tected least significant difference test for comparison of means. $P < 0.05$ was considered to be statistically significant.

Acknowledgments

We are grateful to S. Nishikawa (Center for Developmental Biology, RIKEN, Japan) for providing APA5 hybridoma cells. We thank A. Furuyama, M. Ikeda, Y. Ohtsuki, I. Sakamoto, and M. Kikuchi for their excellent technical assistance. This work was supported in part by grants from the Japanese Ministry of Education, Science, Sports, and Culture, and Health and Labor Sciences Research grants (to I. Komuro and H. Akazawa); and grants from Japan Intractable Diseases Research Foundation and Takeda Science Foundation (to H. Akazawa).

Received for publication May 21, 2009, and accepted in revised form October 14, 2009.

Address correspondence to: Issei Komuro, Department of Cardiovascular Science and Medicine, Chiba University Graduate School of Medicine, 1-8-1 Inohana, Chuo-ku, Chiba 260-8670, Japan. Phone: 81-43-226-2097; Fax: 81-43-226-2557; E-mail: komuro-tky@umin.ac.jp.

1. Fuster V, et al. ACC/AHA/ESC 2006 guidelines for the management of patients with atrial fibrillation. *Circulation.* 2006;114(7):e257–354.
2. Nattel S. New ideas about atrial fibrillation 50 years on. *Nature.* 2002;415(6868):219–226.
3. Burstein B, Nattel S. Atrial fibrosis: mechanisms and clinical relevance in atrial fibrillation. *J Am Coll Cardiol.* 2008;51(8):802–809.
4. Corradi D, Callegari S, Maestri R, Benussi S, Alfieri O. Structural remodeling in atrial fibrillation. *Nat Clin Pract Cardiovasc Med.* 2008;5(12):782–796.
5. Frustaci A, et al. Histological substrate of atrial biopsies in patients with lone atrial fibrillation. *Circulation.* 1997;96(4):1180–1184.
6. Issac TT, Dokainish H, Lakkis NM. Role of inflammation in initiation and perpetuation of atrial fibrillation: a systematic review of the published data. *J Am Coll Cardiol.* 2007;50(21):2021–2028.
7. Nakamura Y, et al. Tissue factor expression in atrial endothelia associated with nonvalvular atrial fibrillation: possible involvement in intracardiac thrombogenesis. *Thromb Res.* 2003;111(3):137–142.
8. Verheule S, et al. Alterations in atrial electrophysiology and tissue structure in a canine model of chronic atrial dilatation due to mitral regurgitation. *Circulation.* 2003;107(20):2615–2622.
9. Chung MK, et al. C-reactive protein elevation in patients with atrial arrhythmias: inflammatory mechanisms and persistence of atrial fibrillation. *Circulation.* 2001;104(24):2886–2891.
10. Aviles RJ, et al. Inflammation as a risk factor for atrial fibrillation. *Circulation.* 2003;108(24):3006–3010.
11. Kalesnikoff J, Galli SJ. New developments in mast cell biology. *Nat Immunol.* 2008;9(11):1215–1223.
12. Metz M, Grimbaldeston MA, Nakae S, Piliponsky AM, Tsai M, Galli SJ. Mast cells in the promotion and limitation of chronic inflammation. *Immunol Rev.* 2007;217:304–328.
13. Sperr WR, et al. The human cardiac mast cell: localization, isolation, phenotype, and functional characterization. *Blood.* 1994;84(11):3876–3884.
14. Bot I, et al. Perivascular mast cells promote atherogenesis and induce plaque destabilization in apolipoprotein E-deficient mice. *Circulation.* 2007;115(19):2516–2525.
15. Sun J, et al. Mast cells promote atherosclerosis by releasing proinflammatory cytokines. *Nat Med.* 2007;13(6):719–724.
16. Sun J, et al. Mast cells modulate the pathogenesis of elastase-induced abdominal aortic aneurysms in mice. *J Clin Invest.* 2007;117(11):3359–3368.
17. Tsuruda T, et al. Adventitial mast cells contribute to pathogenesis in the progression of abdominal aortic aneurysm. *Circ Res.* 2008;102(11):1368–1377.
18. Hara M, et al. Evidence for a role of mast cells in the evolution to congestive heart failure. *J Exp Med.* 2002;195(3):375–381.
19. Higuchi H, et al. Mast cells play a critical role in the pathogenesis of viral myocarditis. *Circulation.* 2008;118(4):363–372.
20. Mackins CJ, et al. Cardiac mast cell-derived renin promotes local angiotensin formation, norepinephrine release, and arrhythmias in ischemia/reperfusion. *J Clin Invest.* 2006;116(4):1063–1070.
21. Cairns JA, Walls AF. Mast cell tryptase stimulates the synthesis of type I collagen in human lung fibroblasts. *J Clin Invest.* 1997;99(6):1313–1321.
22. Kondo S, et al. Role of mast cell tryptase in renal interstitial fibrosis. *J Am Soc Nephrol.* 2001;12(8):1668–1676.
23. Mori R, Shaw TJ, Martin P. Molecular mechanisms linking wound inflammation and fibrosis: knockdown of osteopontin leads to rapid repair and reduced scarring. *J Exp Med.* 2008;205(1):43–51.
24. Theoharides TC, Kempuraj D, Tagen M, Conti P, Kalogeromitros D. Differential release of mast cell mediators and the pathogenesis of inflammation. *Immunol Rev.* 2007;217:65–78.
25. Sano M, et al. p53-induced inhibition of Hif-1 causes cardiac dysfunction during pressure overload. *Nature.* 2007;446(7134):444–448.
26. Tharp MD, Seelig LL Jr, Tigelaar RE, Bergstresser PR. Conjugated avidin binds to mast cell granules. *J Histochem Cytochem.* 1985;33(1):27–32.
27. Zymek P, et al. The role of platelet-derived growth factor signaling in healing myocardial infarcts. *J Am Coll Cardiol.* 2006;48(11):2315–2323.
28. Olgin JE, Verheule S. Transgenic and knockout mouse models of atrial arrhythmias. *Cardiovasc Res.* 2002;54(2):280–286.
29. Kitamura Y, Go S, Hatanaka K. Decrease of mast cells in W/Wv mice and their increase by bone marrow transplantation. *Blood.* 1978;52(2):447–452.
30. Huizinga JD, et al. W/kit gene required for interstitial cells of Cajal and for intestinal pacemaker activity. *Nature.* 1995;373(6512):347–349.
31. Li M, et al. c-kit is required for cardiomyocyte terminal differentiation. *Circ Res.* 2008;102(6):677–685.
32. Lewis JP, O'Grady LF, Bernstein SE, Russell EE, Trobaugh FE, Jr. Growth and differentiation of transplanted W/Wv marrow. *Blood.* 1967;30(5):601–616.
33. Patella V, et al. Stem cell factor in mast cells and increased mast cell density in idiopathic and ischemic cardiomyopathy. *Circulation.* 1998;97(10):971–978.
34. Galli SJ, et al. Mast cells as "tunable" effector and immunoregulatory cells: recent advances. *Annu Rev Immunol.* 2005;23:749–786.
35. Thompson HL, Burbelo PD, Segui-Real B, Yamada Y, Metcalfe DD. Laminin promotes mast cell attachment. *J Immunol.* 1989;143(7):2323–2327.
36. Dastych J, Costa JJ, Thompson HL, Metcalfe DD. Mast cell adhesion to fibronectin. *Immunology.* 1991;73(4):478–484.
37. Bianchine PJ, Burd PR, Metcalfe DD. IL-3-dependent mast cells attach to plate-bound vitronectin. Demonstration of augmented proliferation in response to signals transduced via cell surface vitronectin receptors. *J Immunol.* 1992;149(11):3665–3671.
38. Bonner JC. Regulation of PDGF and its receptors in fibrotic diseases. *Cytokine Growth Factor Rev.* 2004;15(4):255–273.
39. Burstein B, Libby E, Calderone A, Nattel S. Differential behaviors of atrial versus ventricular fibroblasts: a potential role for platelet-derived growth factor in atrial-ventricular remodeling differences. *Circulation.* 2008;117(13):1630–1641.
40. Kumagai K, et al. Effects of angiotensin II type 1 receptor antagonist on electrical and structural remodeling in atrial fibrillation. *J Am Coll Cardiol.* 2003;41(12):2197–2204.
41. Nattel S, Shiroshita-Takeshita A, Brundel BJ, Rivard L. Mechanisms of atrial fibrillation: lessons from animal models. *Prog Cardiovasc Dis.* 2005;48(1):9–28.
42. Suzuki M, et al. Functional roles of cardiac and vascular ATP-sensitive potassium channels clarified by Kir6.2-knockout mice. *Circ Res.* 2001;88(6):570–577.
43. Oka T, et al. Cardiac-specific deletion of Gata4 reveals its requirement for hypertrophy, compensation, and myocyte viability. *Circ Res.* 2006;98(6):837–845.
44. Jensen BM, Swindle EJ, Iwai S, Gilfillan AM. Generation, isolation, and maintenance of rodent mast cells and mast cell lines. In Coligan, JE, Bierer, B, Margulies, DH, Shevach, EM, Strober, W, Coico, R, eds. *Current Protocols in Immunology.* Hoboken, NJ: John Wiley & Sons; 2006:Chapter 3:Unit 3.23.
45. Zou Y, et al. Cell type-specific angiotensin II-evoked signal transduction pathways: critical roles of Gbetagamma subunit, Src family, and Ras in cardiac fibroblasts. *Circ Res.* 1998;82(3):337–345.
46. Takakura N, Yoshida H, Kunisada T, Nishikawa S, Nishikawa SI. Involvement of platelet-derived growth factor receptor-alpha in hair canal formation. *J Invest Dermatol.* 1996;107(5):770–777.

Inhibition of Semaphorin As a Novel Strategy for Therapeutic Angiogenesis

Junji Moriya,* Tohru Minamino,* Kaoru Tateno, Sho Okada, Akiyoshi Uemura, Ippei Shimizu, Masataka Yokoyama, Aika Nojima, Mitsuhiro Okada, Hisashi Koga, Issei Komuro

Rationale: The axon-guiding molecules known as semaphorins and their receptors (plexins) regulate the vascular pattern and play an important role in the development of vascular network during embryogenesis. Semaphorin (Sema)3E is one of the class 3 semaphorins, and plexinD1 is known to be its receptor. Although these molecules have a role in embryonic vascular development, it remains unclear whether the Sema3E/plexinD1 axis is involved in postnatal angiogenesis.

Objective: The objective of this study was to elucidate the role of Sema3E/plexinD1 in postnatal angiogenesis.

Methods and Results: Sema3E inhibited cell growth and tube formation by suppressing the vascular endothelial growth factor (VEGF) signaling pathway. Expression of Sema3E and plexinD1 was markedly upregulated in ischemic limbs of mice (2.5- and 4.5-fold increase for Sema3E and plexinD1, respectively), and inhibition of this pathway by introduction of the plexinD1-Fc gene or disruption of Sema3E led to a significant increase of blood flow recovery (1.6- and 1.5-fold increase for the plexinD1-Fc gene treatment and Sema3E disruption, respectively). Hypoxia activated the tumor suppressor protein p53, thereby upregulating Sema3E expression. Expression of p53 and Sema3E was enhanced in diabetic mice compared with normal mice (2- and 1.3-fold increase for p53 and Sema3E, respectively). Consequently, neovascularization after VEGF treatment was poor in the ischemic tissues of diabetic mice, whereas treatment with VEGF plus plexinD1-Fc markedly improved neovascularization.

Conclusions: These results indicate that inhibition of Sema3E may be a novel strategy for therapeutic angiogenesis, especially when VEGF is ineffective. (*Circ Res.* 2010;106:391-398.)

Key Words: angiogenesis ■ semaphorins ■ p53 ■ diabetes

The vascular system and nervous system have several striking anatomic similarities. Recent findings have shown that the similarities between these systems extend to the molecular level and that the molecular mechanisms which are important for the specification, differentiation, and patterning of nerves also play an important role within the vasculature and vice versa.[1–4] Development of the nervous system is regulated through the coordinated action of a variety of repulsive or attractive neuronal guidance factors, called "axon-guiding molecules," that direct the growth of axons into specific pathways.[3] Recently, these axon-guiding molecules (including semaphorins) have also been shown to play a pivotal role in the formation of vascular networks.[1,5]

Semaphorins and their receptors (known as plexins) were initially characterized as signaling molecules that repel or attract axons,[6–9] but are now recognized as critical regulators of morphogenesis and homeostasis in various organs and systems.[10,11] The semaphorin family comprises 21 genes in vertebrates and eight additional genes are found in invertebrates. These genes are divided into eight classes on the basis of the similarity of their structural domains, with classes 3 to 7 containing the vertebrate semaphorins.[5] Class 3 are the only semaphorins secreted in vertebrates. Semaphorin (Sema)3E is one of the class 3 semaphorins,[12] and plexinD1 is known to be its receptor.[10] It has been reported that loss of plexinD1 or Sema3E causes abnormalities of vascular growth,[10] suggesting that these molecules have a crucial role in regulating the pattern of vessel development during embryogenesis.[13,14] However, it remains unknown whether Sema3E and plexinD1 are involved in postnatal angiogenesis.

Original received February 26, 2009; resubmission received October 7, 2009; revised resubmission received November 11, 2009; accepted November 13, 2009.

This manuscript was sent to Ingrid Fleming, Consulting Editor, for review by expert referees, editorial decision, and final disposition.

From the Department of Cardiovascular Science and Medicine (J.M., T.M., K.T., S.O., I.S., M.Y., A.N., I.K.), Chiba University Graduate School of Medicine, Chiba, Japan; PRESTO (T.M.), Japan Science and Technology Agency, Saitama, Japan; Division of Vascular Biology (A.U.), Department of Physiology and Cell Biology, Kobe University Graduate School of Medicine, Japan; Laboratory for Stem Cell Biology (M.O.), RIKEN Center for Developmental Biology, Kobe, Japan; and Laboratory of Medical Genomics (H.K.), Department of Human Genome Research, Kazusa DNA Research Institute, Chiba, Japan.

*Both authors contributed equally to this work.

Correspondence to Issei Komuro, MD, PhD, Department of Cardiovascular Science and Medicine, Chiba University Graduate School of Medicine, 1-8-1 Inohana, Chuo-ku, Chiba 260-8670, Japan. E-mail komuro-tky@umin.ac.jp

Circulation Research **is available at http://circres.ahajournals.org** **DOI: 10.1161/CIRCRESAHA.109.210815**

Non-standard Abbreviations and Acronyms	
ERK	extracellular signal-regulated kinase
HUVEC	human umbilical vein endothelial cell
Sema	semaphorin
VEGF	vascular endothelial growth factor
VEGFR	vascular endothelial growth factor receptor

In this study, we performed both in vivo and in vitro investigations into the role of Sema3E/plexinD1 in postnatal angiogenesis, and we found that these 2 molecules inhibit angiogenesis by suppressing the vascular endothelial growth factor (VEGF) signaling pathway. Sema3E expression was upregulated in ischemic tissue via a p53-dependent pathway. Its upregulation was further enhanced in a diabetic model, attenuating the effect of VEGF treatment, whereas inhibition of Sema3E markedly improved the response to VEGF. These findings suggest that inhibition of Sema3E may be a novel strategy for therapeutic angiogenesis, especially when VEGF is ineffective.

Methods

Cell Culture

Recombinant human VEGF165 (293-VE), monoclonal antihuman VEGF antibody (MAB293) and recombinant human Sema3E were purchased from R&D Systems (Minneapolis, Minn). PlexinD1 Fc protein was generated by ARK Resource (Kumamoto, Japan). Human umbilical vein endothelial cells (HUVECs) were purchased from BioWhittaker (Walkersville, Md) and cultured according to the instructions of the manufacturer. Endothelial cell proliferation was assessed by determining cell counts after culture in the presence of VEGF165 (50 ng/mL) for 2 days. Retroviral stocks were generated by transient transfection of packaging cell line (PT67, Clontech) and stored at −80°C until use. Human endothelial cells (passage 4 to 6) were plated at 5×10^5 cells per 100-mm-diameter dish 24 hours before infections. For infections, the culture medium was replaced by retroviral stocks supplemented with 8 μg/mL polybrene (Sigma, Tokyo, Japan). Forty-eight hours after infections, the infected cell populations were selected by culture in 0.8 μg/mL puromycin for 4 days. High-titer adenoviral stocks (10^9 pfu) were generated with the Adeno-X Expression System (Clontech) according to the instructions of the manufacturer.

Tube-Formation Assay

The tube-formation assay was performed using a commercially available kit according to the manufacturer's instructions (Kurabo, Osaka, Japan). HUVECs were cultured for 11 days in the presence of VEGF165 (10 ng/mL) and test substances, after which they were fixed at room temperature in 70% ethanol. The fixed cells were then incubated first with mouse antihuman CD31 antibody (1:4000 dilution) for 1 hour and then with a goat anti-mouse IgG alkaline phosphatase–conjugated secondary antibody, which was visualization using 5-bromo-4-chloro-3-indolyl phosphate/nitro blue tetrazolium. Capillary-like tube formation was assessed by photography under an inverted phase contrast microscope at a ×40 magnification. The vessel area was defined as the area of CD31-positive cells / total area, which was estimated by an angiogenesis image analyzer (Kurabo, Osaka, Japan). This assay was performed in triplicate.

Western Blot Analysis

Whole cell lysates were prepared in lysis buffer (10 mmol/L Tris-HCl, pH 8, 140 mmol/L NaCl, 5 mmol/L EDTA, 0.025% NaN3, 1% Triton X-100, 1% deoxycholate, 0.1% SDS, 1 mmol/L PMSF, 5 μg/mL leupeptin, 2 μg/mL aprotinin, 50 mmol/L NaF, and 1 mmol/L Na_2VO_3). The lysates (30 to 50 μg) were resolved by SDS-PAGE. Proteins were transferred to a poly(vinylidene difluoride) membrane (Millipore, Bedford, Mass) and incubated with the primary antibody followed by anti-rabbit IgG–horseradish peroxidase antibody or anti-mouse IgG–horseradish peroxidase antibody or anti-goat IgG–horseradish peroxidase antibody (Jackson, West Grove, Pa). Specific proteins were detected by using enhanced chemiluminescence (Amersham, Buckinghamshire, UK). Immunoprecipitation was performed as described previously.[15] The primary antibodies used for Western blotting were as follows; anti–phospho–extracellular signal-regulated kinase (ERK) antibody (sc-7383), anti-ERK antibody (sc-154-G), anti-pAkt antibody (sc-7985-R), anti-Akt antibody (sc-1618), anti-p53 antibody (sc-126, sc-99), anti-actin antibody (sc-8432), anti–flk-1 antibody (sc-6251), anti-Sema3E antibody (sc-49733) (Santa Cruz Biotechnology, Santa Cruz, Calif), and anti-phosphotyrosine antibody (4G10) (Upstate, Lake Placid, NY). All immunoblotting analyses were performed more than three times.

RNA Analysis

Total RNA (30 μg) was extracted by the guanidinium thiocyanate-phenol chloroform method using RNA zol B (Tel Test, Friendswood, Tex) according to the instructions of the manufacturer. cDNA was prepared using the SuperScript First-Strand Synthesis System for RT-PCR (Invitrogen). Quantitative real-time PCR was performed by using the LightCycler (Roche, Indianapolis, Ind) with the TaqMan Universal ProbeLibrary and the LightCycler Master (Roche) according to the instructions of the manufacturer.

Experimental Animals

The animal experiments were approved by our institutional review board. C57/BL6 mice were purchased from the SLC Japan. All mice used in this study were 8 to 12 weeks old. p53-deficient mice (in C57/BL6 background) were purchased from The Jackson Laboratory (Bar Harbor, Me). For the type 1 diabetic model, mice were treated with an intraperitoneal injection of streptozotocin in 0.1 mol/L sodium citrate (pH 4.5) at a dose of 50 mg/kg body weight for 5 days. Generation and genotyping of Sema3E-deficient mice (in C57/BL6 background) have been described previously.[10]

Hindlimb Ischemia Model

After mice were anesthetized, the proximal part of the femoral artery and the distal portion of the popliteal artery were ligated and stripped out after all side branches were dissected free.[16] For in vivo gene transfer, we exposed thigh muscle by excising the skin and injected the expression vector encoding soluble plexinD1-Fc, VEGF, or Sema3E into the muscle twice after surgery. We analyzed blood flow recovery until day 28 after surgery. Hindlimb perfusion was measured with a laser Doppler perfusion analyzer (Moor Instruments, Devon, UK). Ischemic limb samples were harvested for histology on day 10 after surgery. Vastus and rectus femoris muscle tissues were removed from the ischemic limbs after systemic perfusion with PBS and immediately embedded in OCT compound (Sakura Finetechnical). Then, each specimen was snap frozen in liquid nitrogen and cut into 6 μm sections. The sections were stained with antibodies for CD31 (Pharmingen), plexinD1, or Sema3E (Santa Cruz Biotechnology). Two transverse sections of the entire muscle were photographed digitally at a magnification of ×100 (12 to 16 photographs per mouse), and these photographs were reviewed in a blinded manner. Capillary endothelial cells were identified by immunoreactivity for CD31 and quantified as vessel area (%), which was defined as the area of CD31-positive cells/total area.

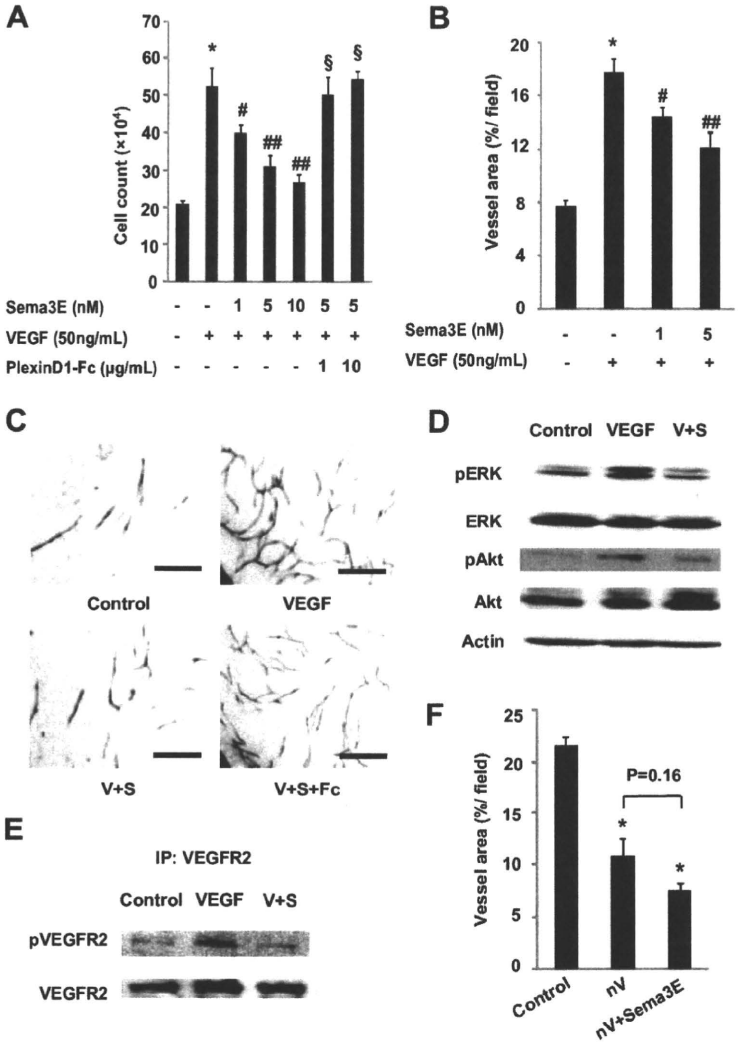

Figure 1. Sema3E suppresses VEGF-induced angiogenesis. A, Cultured endothelial cells were treated with VEGF alone (50 ng/mL) or VEGF+Sema3E (1, 5, or 10 nmol/L) or VEGF+Sema3E+plexinD1-Fc (1 or 10 μg/mL). Sema3E significantly inhibited VEGF-induced endothelial cell proliferation, which was effectively reversed by plexinD1-Fc treatment. *$P<0.01$ vs Sema3E (−)/VEGF (−)/plexinD1-Fc (−) (n=4); #$P<0.05$, ##$P<0.01$ vs Sema3E (−)/VEGF (+)/plexinD1-Fc (−) (n=4); §$P<0.01$ vs Sema3E (5 nmol/L)/VEGF (+)/plexinD1-Fc (−) (n=4). Data represent means±SEM. B, Endothelial cells cocultured with fibroblasts were treated with VEGF and/or Sema3E for 11 days, and vessel area was assayed by immunohistochemistry for CD31. Sema3E significantly inhibited VEGF-induced tube formation. *$P<0.01$ vs Sema3E (−)/VEGF (−) (n=4); #$P<0.05$, ##$P<0.01$ vs Sema3E (−)/VEGF (+) (n=4). Data represent means±SEM. C, Photographs show tube formation of endothelial cells in the presence of VEGF (50 ng/mL) (VEGF), VEGF+Sema3E (5 nmol/L) (V+S), or VEGF+Sema3E+PlexinD1-Fc (10 μg/mL) (V+S+Fc). Scale bar=300 μm. Vehicle treatment served as control (control). D, Endothelial cells were treated with VEGF (50 ng/mL) (VEGF) or VEGF plus Sema3E (5 nmol/L) (V+S) and analyzed for the VEGF signal pathways by Western blot analysis (n=4). Sema3E suppressed VEGF-induced phosphorylation of ERK (pERK) and Akt (pAkt). Vehicle treatment served as control (control). E, Protein samples prepared in D were analyzed for phospho-VEGFR2 levels (n=7). Sema3E suppressed VEGF-induced phosphorylation of VEGFR2. F, VEGF-induced tube formation was examined in the presence of anti-VEGF antibody (500 μg/mL) (nV), Sema3E (5 nmol/L) (Sema3E), or anti-VEGF antibody plus Sema3E (nV+Sema3E). Vehicle treatment served as control (control). In the presence of anti-VEGF antibody, Sema3E did not significantly inhibit tube formation. *$P<0.01$ vs control (n=4).

Statistical Analysis

Data were shown as means±SEM. Multiple group comparison was performed by 1-way ANOVA followed by the Bonferroni procedure for comparison of means. Comparisons between 2 groups were analyzed by the unpaired Student *t* test. Values of $P<0.05$ were considered statistically significant.

Results

Sema3E Suppresses VEGF-Induced Angiogenesis in Cultured Endothelial Cells

To investigate the role of Sema3E/plexinD1, we first performed an in vitro study using HUVECs. We seeded HUVECs at 1×10^5 cells per 100-mm-diameter dish and counted the number of cells at 2 days after seeding. Treatment of HUVECs with VEGF markedly increased the cell count (Figure 1A), although this increase was strongly inhibited by addition of Sema3E in a dose-dependent manner (Figure 1A). Treatment with a plexinD1-Fc fusion protein, which binds to Sema3E and inhibits its activity, blocked the effect of Sema3E (Figure 1A). We also performed an angiogenesis assay, in which HUVECs were cocultured with fibroblasts in the presence or absence of Sema3E. When endothelial tube formation was assessed after 11 days, it was found that treatment with VEGF markedly increased tube formation, although this increase was significantly inhibited by addition of Sema3E (Figure 1B). Treatment with the plexinD1-Fc fusion protein also antagonized the effect of Sema3E on VEGF-induced tube formation (Figure 1C), suggesting that Sema3E is an antiangiogenic factor. We next investigated how Sema3E inhibited angiogenesis. After depriving HUVECs of VEGF for 7 hours, we examined the effect of VEGF treatment. Addition of VEGF induced the phosphorylation of ERK and Akt, both of which are crucial kinases in the intracellular signaling pathway for this growth factor. Pretreatment with Sema3E suppressed VEGF-induced phosphorylation of these two kinases (Figure 1D; Online Figure I, A). Sema3E treatment also suppressed VEGF-induced phosphorylation of VEGF receptor (VEGFR)-2 (Figure 1E; Online Figure I, B). To determine whether the antiangiogenic effect of Sema3E was VEGF-dependent, we next examined the response to addition of an anti-VEGF neutralizing antibody. In the presence of the anti-VEGF antibody, Sema3E did not significantly inhibit cell growth and tube formation (Figure 1F; Online Figure I, C),

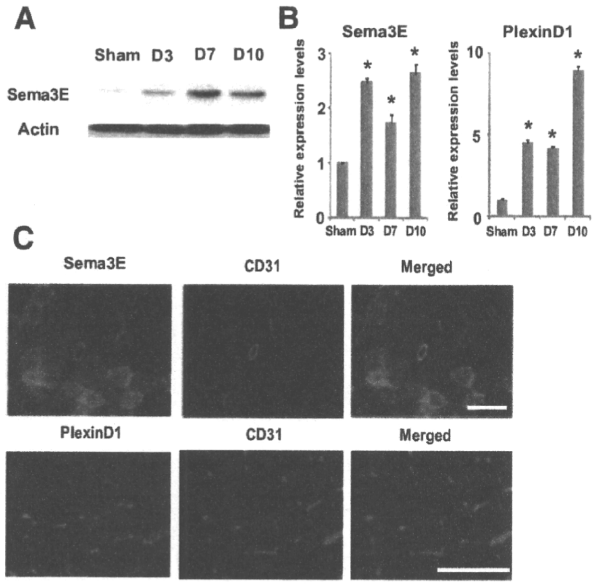

Figure 2. Expression of Sema3E is markedly upregulated in ischemic tissues. A, Western blot analysis for Sema3E expression in ischemic limbs on day 3 (D3), day 7 (D7), and day 10 (D10) after surgery (n=5). Sham indicates sham-operated. B, The mRNA levels of Sema3E and plexinD1 in ischemic limbs on day 3 (D3), day 7 (D7), and day 10 (D10) after surgery were assessed by real-time PCR analysis. *$P<0.01$ vs sham (n=5). Data represent means±SEM. C, The frozen sections of murine ischemic tissue on day 10 after surgery were subjected to immunofluorescence staining for Sema3E (top) or plexinD1 (bottom) (green). The sections were double-stained with CD31 (red). Scale bar=100 μm.

suggesting that Sema3E negatively regulates angiogenesis by inhibiting the VEGF pathway.

Sema3E Suppresses Angiogenesis In Vivo

To investigate the role of Sema3E/plexinD1 in postnatal angiogenesis, we used a murine model of hindlimb ischemia that was created by unilateral femoral artery ligation. Ischemic tissues were harvested and subjected to Western blot analysis and immunohistochemistry. Expression of Sema3E and plexinD1 was markedly increased in ischemic limbs at 3 days after surgery, and this increase persisted until day 10 (Figure 2A and 2B; Online Figure II). Immunohistochemistry showed that Sema3E was expressed by arterioles, myocytes, and capillary endothelial cells in the ischemic limbs, whereas plexinD1 was mainly expressed by capillary endothelial cells (Figure 2C). To examine whether inhibition of Sema3E promoted angiogenesis, we injected an expression vector encoding the plexinD1-Fc gene into ischemic limbs and analyzed blood flow recovery and the vessel area of the limbs. Laser Doppler perfusion imaging revealed that the plexinD1-Fc group showed significantly better recovery of blood flow than the control group (Figure 3A). Likewise, the vessel area of ischemic limbs at 10 days after surgery was significantly larger in the plexinD1-Fc group than in the control group (Figure 3B; Online Figure III, A).

To further investigate the effect of Sema3E on angiogenesis, we introduced an expression vector encoding the VEGF gene, a vector for the Sema3E gene, or the vectors for both genes. Injection of the VEGF vector into ischemic limbs significantly accelerated blood flow recovery compared with the control group, whereas this effect was suppressed by coinjection of the Sema3E vector (Figure 3C). In addition, the vessel area was smaller in the Sema3E plus VEGF group than in the VEGF alone group (Figure 3C). Moreover, injection of a vector encoding the plexinD1-Fc gene into ischemic limbs treated with the Sema3E and VEGF vectors significantly improved blood flow recovery and increased the vessel area compared with the findings in the Sema3E plus VEGF group (Figure 3C), suggesting that Sema3E also inhibits neovascularization in ischemic tissue. Next, we created hindlimb ischemia in Sema3E-deficient mice to examine the effect of loss-of-function of this molecule. Consistent with the results of our gene transfer experiments, Sema3E-deficient mice[10] showed better blood flow recovery and a larger vessel area in their ischemic limbs than wild-type mice (Figure 3D; Online Figure III, B). These results indicate that Sema3E/plexinD1 negatively regulate postnatal angiogenesis.

p53 Upregulates Sema3E Expression Both In Vitro and In Vivo

There is evidence that expression of the tumor suppressor protein p53 is increased by hypoxia, thereby inhibiting tumor angiogenesis.[17,18] We identified a putative p53-binding element within the promoter region of the Sema3E gene (data not shown), suggesting that induction of p53 by hypoxia might upregulate Sema3E expression in ischemic limbs. To investigate this hypothesis, we infected HUVECs with an adenoviral vector encoding p53, and then examined Sema3E expression by Western blot analysis. In agreement with our hypothesis, overexpression of p53 led to upregulation of Sema3E expression in HUVECs (Figure 4A). Expression of Sema3E was also induced by treatment with cobalt chloride, which mimics the effects of hypoxia (Figure 4B). To further investigate the relationship between p53 and Sema3E, we next infected HUVECs with a retroviral vector encoding the HPV16 E6 gene, which blocks p53 expression and examined the effect on expression of Sema3E by endothelial cells. Exposure to cobalt chloride for 12 hours markedly upregulated both Sema3E and p53 expression in mock-infected HUVECs, whereas there was no induction of Sema3E expression in E6-infected cells (Figure 4B), suggesting that hypoxia promoted the induction of Sema3E via a p53-dependent pathway.

Consistent with our in vitro data, expression of both p53 and Sema3E was markedly increased in the ischemic limbs of wild-type mice at 3 days after femoral artery ligation (Figures 2A and 4C; Online Figure IV, A). To determine whether Sema3E was regulated by p53 in vivo, we created hindlimb ischemia in p53-deficient mice and wild-type mice and then examined the expression of Sema3E in ischemic limbs. Consistent with our in vitro results, upregulation of Sema3E expression was abolished in the ischemic limbs of p53-deficient mice (Figure 4D; Online Figure IV, B), suggesting that an increase of p53 promotes Sema3E expression in ischemic tissue and thus inhibits blood flow recovery.

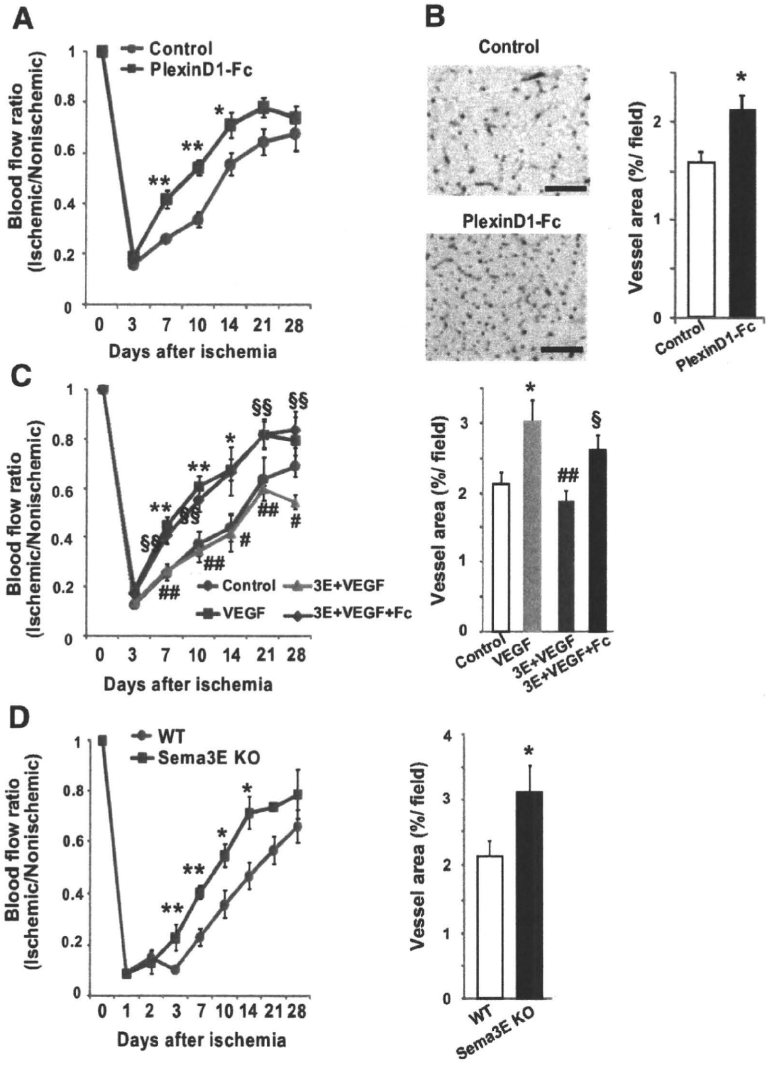

Figure 3. Sema3E negatively regulates angiogenesis in ischemic tissue. A and B, Ischemic limbs of mice were treated with an empty vector (control) or the plexinD1-Fc expression vector (plexinD1-Fc) by intramuscular injection, and blood flow recovery (A) and vessel area (B) were analyzed by laser Doppler perfusion imaging and immunohistochemistry for CD31, respectively. Mice treated with plexinD1-Fc showed better blood flow recovery and a larger vessel area. *$P<0.05$, **$P<0.01$ vs control (n=8 for A and B). Data represent means±SEM. Photographs show immunohistochemistry for CD31 in ischemic limbs on 10 days after surgery. Scale bar=100 μm. C, Ischemic limbs of mice were treated with mock (control), the VEGF vector only (VEGF), the Sema3E and VEGF vectors (3E+VEGF), or the Sema3E, VEGF, and plexinD1-Fc vectors (3E+VEGF+Fc), and blood flow recovery (left) and vessel area (right) were analyzed by laser Doppler perfusion imaging and CD31 immunohistochemistry, respectively. Injection of the Sema3E vector into ischemic limbs suppressed VEGF-induced neovascularization, which was effectively reversed by the plexinD1-Fc vector treatment. *$P<0.05$, **$P<0.01$ vs control; #$P<0.05$, ##$P<0.01$ vs VEGF; §$P<0.05$, §§$P<0.01$ vs 3E+VEGF (n=8 to 10). Data represent means±SEM. D, Ischemic limbs of wild-type mice (WT) and Sema3E-deficient mice (Sema3E KO) were analyzed for blood flow recovery (left) and vessel area (right). Sema3E-deficient mice showed better blood flow recovery and a larger vessel area of ischemic limbs. *$P<0.05$ vs WT mice (n=3 to 8). Data represent means±SEM.

Inhibition of Sema3E Improves Angiogenesis in Diabetic Mice

It has been reported that the angiogenic response to ischemia is attenuated in patients with diabetes.[19] We created a murine model of type 1 diabetes by intraperitoneal injection of streptozotocin (50 mg/kg per day for 5 days) and examined neovascularization after the animals were subjected to hind-limb ischemia. Blood glucose level was significantly higher and blood insulin level was significantly lower in streptozotocin-induced diabetic mice than in control mice (Online Figure V, A). Mice with streptozotocin-induced diabetes also showed poor blood flow recovery and a smaller vessel area in their ischemic limbs compared with control mice (Figure 5A and 5B). To investigate whether the impairment of neovascularization in diabetic mice was related to p53 and Sema3E, we examined the expression of these proteins in the mice. Western blot analysis revealed that p53 expression was increased in diabetic mice and that this increase was further enhanced by ischemia (Figure 5C; Online Figure V, B; and data not shown). Likewise, expression of Sema3E was significantly increased in diabetic mice compared with control mice (Figure 5C; Online Figure V, B). Consequently, blood flow recovery and the increase of the vessel area after VEGF treatment were significantly impaired in diabetic mice compared with VEGF-treated control mice (Figure 5A and 5B). To further assess the effect of inhibition of Sema3E in diabetic mice, we injected an expression vector encoding the plexinD1-Fc gene into the ischemic limbs of diabetic mice. Laser Doppler perfusion imaging of ischemic limbs and immunohistochemistry for CD31 revealed that the poor response of neovascularization to VEGF treatment was effectively overcome by introduction of the plexinD1-Fc gene (Figure 5D), suggesting that overexpression of Sema3E was responsible for impairment of neovascularization in the diabetic mice. These results indicate that inhibition of Sema3E is effective for promoting angiogenesis, especially when VEGF treatment is ineffective, such as in the diabetic state.

Discussion

The present study demonstrated that the Sema3E/plexinD1 axis inhibits postnatal angiogenesis in a murine model of

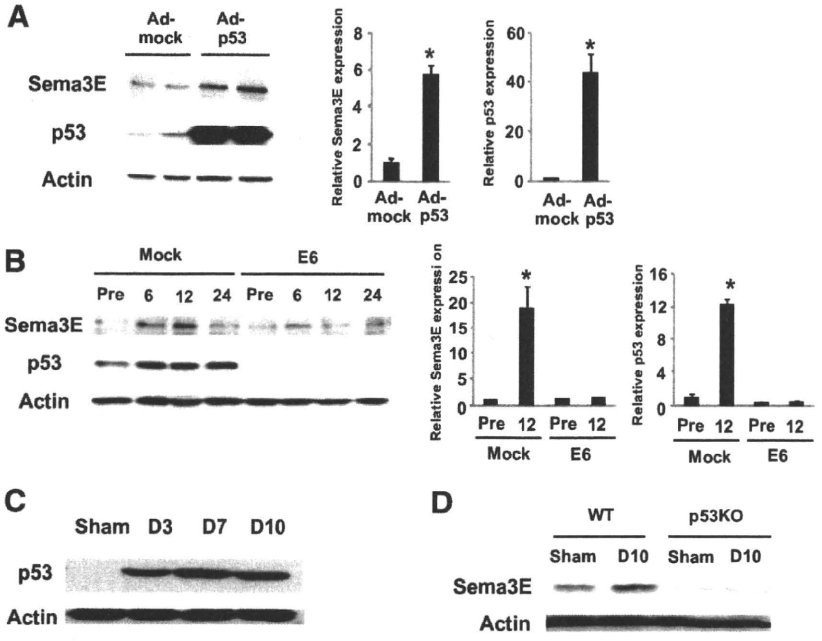

Figure 4. p53 regulates expression of Sema3E. A, Endothelial cells were infected with an adenoviral vector encoding p53 (Ad-p53) or mock (Ad-mock) and subjected to Western blot analysis for expression of Sema3E and p53 (left). Relative expression levels of Sema3E and p53 were plotted in the graph (right). *$P<0.01$ vs Ad-mock (n=4). Overexpression of p53 upregulated Sema3E expression. B, Endothelial cells were infected with a retroviral vector encoding HPV16 E6 (E6) or mock (Mock) and treated with $CoCl_2$ (100 μmol/L) for 6, 12, 24 hours (6, 12, 24). Expression of Sema3E and p53 was examined by Western blot analysis (left). Relative expression levels of Sema3E and p53 were plotted in the graph (right). *$P<0.05$ vs control (Pre) (n=3). Treatment with $CoCl_2$ markedly upregulated Sema3E expression compared to control (Pre), and this upregulation was inhibited by disruption of p53. C, Western blot analysis for p53 expression on day 3 (D3), day 7 (D7), and day 10 (D10) after surgery (n=4). Sham indicates sham-operated. Expression of p53 was markedly upregulated 3 days after surgery, and this upregulation persisted for 10 days. D, Western blot analysis for Sema3E expression in ischemic limbs of wild-type (WT) or p53-deficient (p53KO) mice on day 10 after surgery (n=4). Sema3E expression was increased in ischemic limbs of wild-type mice but not p53-deficient mice.

hindlimb ischemia. Our results also suggested that Sema3E inhibits angiogenesis by blocking activation of the VEGFR-2 and its downstream signaling pathway. Although Sema3E does not bind to neuropilin-1,[10] attraction of axons by Sema3E requires the presence of neuropilin-1 in addition to plexinD1, so the mode of assembly of the ligand and receptor complex is thought to determine the function of Sema3E.[20] Neuropilin-1 also binds to the VEGFR-2 and plays a crucial role in the regulation of VEGF signaling.[21] Accordingly, Sema3E may inhibit VEGF-induced angiogenesis by limiting the availability of neuropillin-1. Because treatment with an anti-VEGF neutralizing antibody did not completely over-

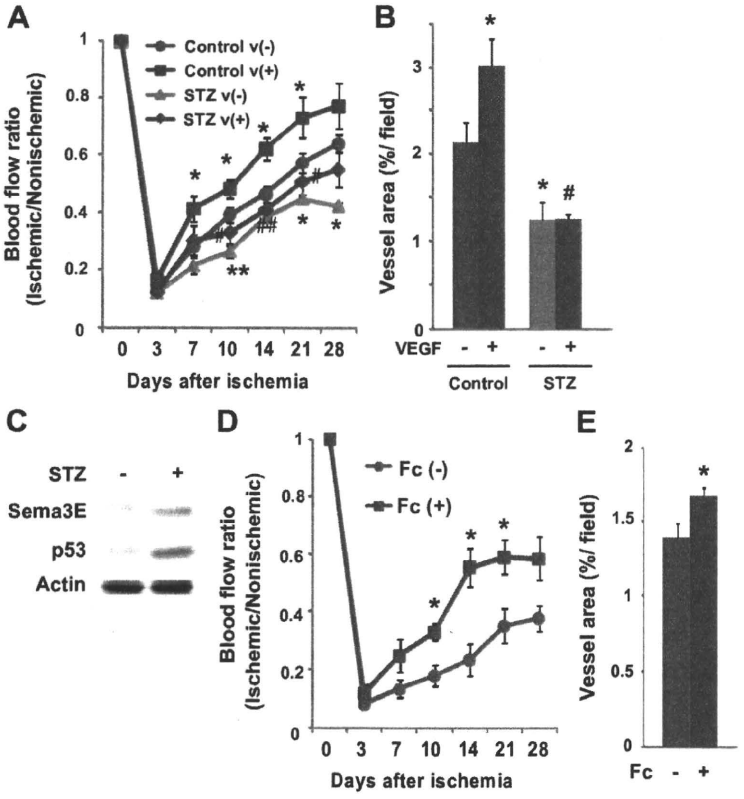

Figure 5. Sema3E inhibition improves impaired angiogenesis in diabetic mice. A and B, Blood flow recovery (A) and vessel area (B) in ischemic limbs of control (control) or streptozotocin-induced diabetic (STZ) mice after treatment with mock [v(−)] or the VEGF expression vector [v(+)]. Diabetic mice showed impaired blood recovery and a smaller vessel area in ischemic limbs compared with control mice. They showed less response to VEGF treatment. *$P<0.05$, **$P<0.01$ vs control/v(−); #$P<0.05$, ##$P<0.01$ vs control/v(+) (n=5 to 12). Data represent means±SEM. C, Expression of Sema3E and p53 was examined in limb tissues of control (STZ−) and streptozotocin-induced diabetic mice (STZ+) by Western blot analysis (n=4). Expression of Sema3E and p53 was upregulated in diabetic mice. D and E, Blood flow recovery (D) and vessel area (E) were analyzed in ischemic limbs of diabetic mice treated with VEGF [Fc(−)] or VEGF+plexinD1-Fc [Fc(+)]. Treatment of plxinD1-Fc in addition to VEGF significantly improved neovascularization in diabetic mice. *$P<0.01$ vs Fc(−) (n=7 to 9). Data represent means±SEM.

come the inhibitory effect of Sema3E on angiogenesis, this effect may also be attributable to the signaling pathway downstream of Sema3E-plexinD1, which is currently unknown.

Sema3E suppressed VEGF-induced phosphorylation of ERK and Akt (Figure 1D). It is well accepted that both ERK and Akt are crucial for the intracellular signaling pathways stimulated by hepatocyte growth factor (HGF) or basic fibroblast growth factor basic (bFGF) to induce angiogenesis. Interestingly, Sema3E also inhibited bFGF or HGF-induced tube formation in a dose-dependent manner (Online Figure VI, A). Moreover, Sema3E significantly inhibited bFGF-induced tube formation even in the presence of the anti-VEGF antibody, whereas it did not inhibit HGF-induced tube formation (Online Figure VI, B). These results suggest that besides the suppression of VEGF-induced angiogenesis, the antiangiogenic effect of Sema3E was partially mediated by VEGF-independent mechanisms.

It is known that intersomitic vessels are disorganized in Sema3E-deficient mice,[10] and this phenotype is markedly similar to that observed in mice lacking plexinD1.[13,14] However, whereas plexinD1-deficient mice develop severe cardiovascular defects involving the outflow tract of the heart and derivatives of the aortic arch arteries that result in perinatal death,[13] Sema3E-deficient mice do not show any large vessel abnormalities and do not undergo embryonic death. PlexinD1 has also been reported to bind to other semaphorins besides Sema3E, such as Sema3A,[13] Sema3C,[22] and Sema4A.[23] It has been shown that Sema3E only binds to plexinD1, whereas Sema3A and Sema3C bind to plexinA1 as well as to plexinD1.[5,10] Sema3A-deficient mice show neural path-finding defects and abnormalities of vascular development that result in neonatal death.[24–26] Ablation of the Sema3C gene in mice results in severe outflow tract abnormalities and mispatterning of intersomitic vessels.[27] Because plexinA1 deficiency also leads to cardiovascular defects,[28] Sema3A/C may play a pivotal role in embryonic vascular development regulated by the plexinA1/D1 pathway. More recently, Sema3A and Sema4A have been shown to inhibit postnatal angiogenesis,[29] suggesting that plexinD1-Fc treatment increases blood flow recovery in ischemic limbs by inhibiting Sema3E but also Sema3A/4A. Sema4D also has an inhibitory effect on postnatal angiogenesis[30]; however, it remains to be determined whether Sema4D binds to plexinD1.

Our results further suggest that p53 has a crucial role in the induction of Sema3E expression in ischemic tissue, although the precise mechanism of how p53 regulates Sema3E expression remains unknown. Because the antiangiogenic activity of p53 is important for tumor suppression, Sema3E/plexinD1 could be a potential target for the treatment of malignancies with p53 mutations. It has been reported that hyperglycemia activates p53 by increasing the production of reactive oxygen species.[31] Thus, p53-induced upregulation of antiangiogenic factors (including Sema3E) is likely to account for the impairment of angiogenesis in patients with diabetes. Therefore, Sema3E/plexinD1 could also be a target for the treatment of ischemic cardiovascular disease in diabetic patients because conventional therapeutic angiogenesis is not very efficient in this patient population.[32,33]

Acknowledgment

We thank Christopher Henderson, Columbia University, New York, for providing us with Sema3E knockout mice.

Sources of Funding

This work was supported by a Grant-in-Aid for Scientific Research from the Ministry of Education, Science, Sports, and Culture and Health and Labor Sciences Research Grants (to I.K.); a Grant-in-Aid for Scientific Research from the Ministry of Education, Culture, Sports, Science and Technology of Japan and grants from the Suzuken Memorial Foundation, the Japan Diabetes Foundation, the Ichiro Kanehara Foundation, the Tokyo Biochemical Research Foundation, the Takeda Science Foundation, the Cell Science Research Foundation, and the Japan Foundation of Applied Enzymology (to T.M.).

Disclosures

None.

References

1. Carmeliet P, Tessier-Lavigne M. Common mechanisms of nerve and blood vessel wiring. *Nature*. 2005;436:193–200.
2. Dickson BJ. Molecular mechanisms of axon guidance. *Science*. 2002; 298:1959–1964.
3. Weinstein BM. Vessels and nerves: marching to the same tune. *Cell*. 2005;120:299–302.
4. Eichmann A, Le Noble F, Autiero M, Carmeliet P. Guidance of vascular and neural network formation. *Curr Opin Neurobiol*. 2005;15:108–115.
5. Neufeld G, Kessler O. The semaphorins: versatile regulators of tumour progression and tumour angiogenesis. *Nat Rev Cancer*. 2008;8:632–645.
6. Luo Y, Raible D, Raper JA. Collapsin: a protein in brain that induces the collapse and paralysis of neuronal growth cones. *Cell*. 1993;75:217–227.
7. Tamagnone L, Artigiani S, Chen H, He Z, Ming GI, Song H, Chedotal A, Winberg ML, Goodman CS, Poo M, Tessier-Lavigne M, Comoglio PM. Plexins are a large family of receptors for transmembrane, secreted, and GPI-anchored semaphorins in vertebrates. *Cell*. 1999;99:71–80.
8. Ohta K, Mizutani A, Kawakami A, Murakami Y, Kasuya Y, Takagi S, Tanaka H, Fujisawa H. Plexin: a novel neuronal cell surface molecule that mediates cell adhesion via a homophilic binding mechanism in the presence of calcium ions. *Neuron*. 1995;14:1189–1199.
9. Song H, Ming G, He Z, Lehmann M, McKerracher L, Tessier-Lavigne M, Poo M. Conversion of neuronal growth cone responses from repulsion to attraction by cyclic nucleotides. *Science*. 1998;281:1515–1518.
10. Kruger RP, Aurandt J, Guan KL. Semaphorins command cells to move. *Nat Rev Mol Cell Biol*. 2005;6:789–800.
11. Roth L, Koncina E, Satkauskas S, Cremel G, Aunis D, Bagnard D. The many faces of semaphorins: from development to pathology. *Cell Mol Life Sci*. 2009;66:649–666.
12. Christensen CR, Klingelhofer J, Tarabykina S, Hulgaard EF, Kramerov D, Lukanidin E. Transcription of a novel mouse semaphorin gene, M-semaH, correlates with the metastatic ability of mouse tumor cell lines. *Cancer Res*. 1998;58:1238–1244.
13. Gitler AD, Lu MM, Epstein JA. PlexinD1 and semaphorin signaling are required in endothelial cells for cardiovascular development. *Dev Cell*. 2004;7:107–116.
14. Torres-Vazquez J, Gitler AD, Fraser SD, Berk JD, Van NP, Fishman MC, Childs S, Epstein JA, Weinstein BM. Semaphorin-plexin signaling guides patterning of the developing vasculature. *Dev Cell*. 2004;7:117–123.
15. Minamino T, Mitsialis SA, Kourembanas S. Hypoxia extends the life span of vascular smooth muscle cells through telomerase activation. *Mol Cell Biol*. 2001;21:3336–3342.
16. Couffinhal T, Silver M, Zheng LP, Kearney M, Witzenbichler B, Isner JM. Mouse model of angiogenesis. *Am J Pathol*. 1998;152:1667–1679.
17. Harris SL, Levine AJ. The p53 pathway: positive and negative feedback loops. *Oncogene*. 2005;24:2899–2908.
18. Teodoro JG, Parker AE, Zhu X, Green MR. p53-mediated inhibition of angiogenesis through up-regulation of a collagen prolyl hydroxylase. *Science*. 2006;313:968–971.

19. Falanga V. Wound healing and its impairment in the diabetic foot. *Lancet*. 2005;366:1736–1743.
20. Chauvet S, Cohen S, Yoshida Y, Fekrane L, Livet J, Gayet O, Segu L, Buhot MC, Jessell TM, Henderson CE, Mann F. Gating of Sema3E/PlexinD1 signaling by neuropilin-1 switches axonal repulsion to attraction during brain development. *Neuron*. 2007;56:807–822.
21. Soker S, Takashima S, Miao HQ, Neufeld G, Klagsbrun M. Neuropilin-1 is expressed by endothelial and tumor cells as an isoform-specific receptor for vascular endothelial growth factor. *Cell*. 1998;92:735–745.
22. Banu N, Teichman J, Dunlap-Brown M, Villegas G, Tufro A. Semaphorin 3C regulates endothelial cell function by increasing integrin activity. *FASEB J*. 2006;20:2150–2152.
23. Toyofuku T, Yabuki M, Kamei J, Kamei M, Makino N, Kumanogoh A, Hori M. Semaphorin-4A, an activator for T-cell-mediated immunity, suppresses angiogenesis via Plexin-D1. *EMBO J*. 2007;26:1373–1384.
24. Behar O, Golden JA, Mashimo H, Schoen FJ, Fishman MC. Semaphorin III is needed for normal patterning and growth of nerves, bones and heart. *Nature*. 1996;383:525–528.
25. Taniguchi M, Yuasa S, Fujisawa H, Naruse I, Saga S, Mishina M, Yagi T. Disruption of semaphorin III/D gene causes severe abnormality in peripheral nerve projection. *Neuron*. 1997;19:519–530.
26. Serini G, Valdembri D, Zanivan S, Morterra G, Burkhardt C, Caccavari F, Zammataro L, Primo L, Tamagnone L, Logan M, Tessier-Lavigne M, Taniguchi M, Puschel AW, Bussolino F. Class 3 semaphorins control vascular morphogenesis by inhibiting integrin function. *Nature*. 2003;424:391–397.
27. Feiner L, Webber AL, Brown CB, Lu MM, Jia L, Feinstein P, Mombaerts P, Epstein JA, Raper JA. Targeted disruption of semaphorin 3C leads to persistent truncus arteriosus and aortic arch interruption. *Development*. 2001;128:3061–3070.
28. Toyofuku T, Zhang H, Kumanogoh A, Takegahara N, Suto F, Kamei J, Aoki K, Yabuki M, Hori M, Fujisawa H, Kikutani H. Dual roles of Sema6D in cardiac morphogenesis through region-specific association of its receptor, Plexin-A1, with off-track and vascular endothelial growth factor receptor type 2. *Genes Dev*. 2004;18:435–447.
29. Maione F, Molla F, Meda C, Latini R, Zentilin L, Giacca M, Seano G, Serini G, Bussolino F, Giraudo E. Semaphorin 3A is an endogenous angiogenesis inhibitor that blocks tumor growth and normalizes tumor vasculature in transgenic mouse models. *J Clin Invest*. 2009;119:3356–3372.
30. Sun Q, Zhou H, Binmadi NO, Basile JR. Hypoxia inducible factor-1-mediated regulation of Semaphorin 4D affects tumor growth and vascularity. *J Biol Chem*. 2009;284:32066–32074.
31. Brodsky SV, Gealekman O, Chen J, Zhang F, Togashi N, Crabtree M, Gross SS, Nasjletti A, Goligorsky MS. Prevention and reversal of premature endothelial cell senescence and vasculopathy in obesity-induced diabetes by ebselen. *Circ Res*. 2004;94:377–384.
32. Losordo DW, Dimmeler S. Therapeutic angiogenesis and vasculogenesis for ischemic disease. Part I: angiogenic cytokines. *Circulation*. 2004;109:2487–2491.
33. Losordo DW, Dimmeler S. Therapeutic angiogenesis and vasculogenesis for ischemic disease. Part II: cell-based therapies. *Circulation*. 2004;109:2692–2697.

Circulation Journal
Official Journal of the Japanese Circulation Society
http://www.j-circ.or.jp

REVIEW FOR THE 2009 SATO AWARD

Role of Cellular Senescence in Lifestyle-Related Disease

Tohru Minamino, MD, PhD

Epidemiological studies have shown that age is the chief risk factor for lifestyle-related diseases such as cardiovascular disease and diabetes, but the molecular mechanisms that underlie the increase in the risk of such diseases conferred by aging remain unclear. Recently, genetic analyses using various animal models have identified molecules that are crucial for aging. These include components of the DNA repair system, the tumor suppressor pathway, the telomere maintenance system, the insulin/Akt pathway, and other metabolic pathways. Interestingly, most of the molecules that influence the phenotypic changes of aging also regulate cellular senescence, suggesting a causative link between cellular senescence and aging. This review examines the hypothesis that cellular senescence might contribute to lifestyle-related disease. (*Circ J* 2010; **74:** 2527–2533)

Key Words: Atherosclerosis; Heart failure; Insulin resistance; p53; Telomeres

Vascular Cell Senescence

Vascular cells have a finite lifespan in vitro and eventually enter a state of irreversible growth arrest called cellular senescence. Flattening and enlargement of vascular cells are their morphological characteristics of senescence.[1] Expression of negative regulators of the cell cycle (such as p53 and p16) increases with cell division and thereby promotes growth arrest.[2] Primary cultured cells that undergo senescence in vitro also show increased expression of β-galactosidase (β-gal) activity at pH 6, which is distinguishable from the endogenous lysosomal β-gal activity that can be detected at pH 4. The activity at pH 6 is known as senescence-associated β-gal (SAβ-gal) activity, and because it shows a correlation with the aging of cells it is regarded as a biomarker of cellular senescence.[3] The in vitro growth of vascular cells obtained from human atherosclerotic plaques is impaired, and such cells develop senescence earlier than cells harvested from normal vessels.[4,5] The histology of human atherosclerotic lesions has been extensively studied, and it has been demonstrated that both vascular endothelial cells (ECs) and vascular smooth muscle cells (VSMCs) exhibit the morphological features of cellular senescence,[6,7] which suggests the occurrence of vascular cell senescence in vivo.

In fact, this hypothesis has been confirmed by in vivo cytochemical analysis of SAβ-gal activity. Fenton et al detected SAβ-gal-positive vascular cells in damaged rabbit carotid arteries.[8] After repeated endothelial denudation, accumulation of SAβ-gal-positive cells was markedly enhanced. My group have previously demonstrated SAβ-gal-positive vascular cells in atherosclerotic plaques obtained from the coronary arteries of patients with ischemic heart disease.[9] These SAβ-gal-positive cells were predominately localized on the luminal surface of the atherosclerotic plaques and were identified as ECs, but in the same patients such cells were not observed in the internal mammary arteries where atherosclerotic changes were minimal. In advanced plaques, however, SAβ-gal-positive VSMCs have been detected in the intima and not in the media (**Figure 1**),[10,11] which may have been related to extensive cell replication in the lesions, as is observed in arteries subjected to double denudation. SAβ-gal-positive cells in human atheroma exhibit increased expression of p53 and p16, which is further evidence in favor of in vivo senescence. These cells also show various functional abnormalities, such as decreased expression of endothelial nitric oxide synthase (eNOS) and increased expression of pro-inflammatory molecules.[10,12] Thus, cellular senescence may contribute to the pathogenesis of vascular aging in humans.

Telomere Shortening in Aged Arteries

Telomeres are non-nucleosomal DNA-protein complexes located at the ends of chromosomes, serving as protective caps and acting as the substrate for specialized replication mechanisms. As a consequence of semiconservative DNA replication, the extreme terminals of the chromosomes are not duplicated completely, resulting in successive shortening of the telomeres with each cell division. Telomerase is an enzyme that adds telomeres to the ends of chromosomes.[13] In contrast to stem cells, which have high telomerase activity and maintain telomere length, most somatic cells, including vascular cells, show progressive telomere shortening because of low telomerase activity. Critically short telomeres resemble damaged DNA and thus trigger cellular senescence via a p53-dependent pathway.[14] Recent studies have demonstrated that nuclear foci that contain markers of double-strand DNA

Received September 9, 2010; accepted October 19, 2010; released online November 12, 2010
Department of Cardiovascular Science and Medicine, Chiba University Graduate School of Medicine, Chiba; PRESTO, Japan Science and Technology Agency, Saitama, Japan
Mailing address: Tohru Minamino, MD, PhD, Department of Cardiovascular Science and Medicine, Chiba University Graduate School of Medicine, 1-8-1 Inohana, Chuo-ku, Chiba 260-8670, Japan. E-mail: t_minamino@yahoo.co.jp
ISSN-1346-9843 doi:10.1253/circj.CJ-10-0916